

An error model for instantaneous satellite rainfall estimates: evaluation of BRAIN-TMI over West Africa

Pierre-Emmanuel Kirstetter,^{a*} Nicolas Viltard^a and Marielle Gosset^b

^aUniversité Versailles St-Quentin; CNRS/INSU, LATMOS-IPSL, Guyancourt, France

^bIRD, GET-OMP (IRD, CNRS, Université Toulouse 3), Toulouse, France

*Correspondence to: P.-E. Kirstetter, Instituto Nacional de Pesquisas Espaciais–INPE, Centro de Previsão de Tempo e Estudos Climáticos–CPTEC, Rod. Dutra, km 40–Cachoeira Paulista, Cachoeira Paulista, SP 12630000, Brazil.

E-mail: pierre-emmanuel.kirstetter@latmos.ipsl.fr

Characterising the error associated with satellite rainfall estimates based on spaceborne passive and active microwave measurements is a major issue for many applications, such as water budget studies or assessment of natural hazards caused by extreme rainfall events. We focus here on the error structure of the Bayesian Rain retrieval Algorithm Including Neural Network (BRAIN), the algorithm that provides instantaneous quantitative precipitation estimates at the surface based on the MADRAS radiometer on board the Megha-Tropiques satellite. A version of BRAIN using data from the Tropical Rainfall Measuring Mission (TRMM) Microwave Imager (TMI) has been compared to reference values derived either from TRMM Precipitation Radar (PR) or from a ground validation (GV) dataset. The ground-based measurements were provided by two densified rain-gauge networks in West Africa, using a geostatistical framework. The comparisons were carried out at the BRAIN retrieval scale for TMI (instantaneous and 12.5 km) and over a ten-year-long period. The primary contribution of this study is to provide some insight into the most significant error sources of satellite rainfall retrieval. This involves comparisons of rainfall detectability, distributions and spatial representativeness, as well as separation of systematic biases and random errors using Generalized Additive Models for Location, Scale and Shape. In spite of their different sampling properties, the three rain estimates were found to detect rainfall consistently. The most important BRAIN-TMI error is due to the rain/no-rain delimitation which causes about 20% of volume rainfall loss relative to PR and GV. BRAIN-TMI presents a narrow PDF relative to GV and catches the spatial structure of the most active part of rain fields. The conditional bias is significant (e.g. +2 mm h⁻¹ for light-moderate rain rates, -2 mm h⁻¹ for rain rates greater than 8 mm h⁻¹) and the overall bias is within 10%. The PR shows a significant underestimation for high rain rates with respect to GV. The proposed framework could be applied to the evaluation of other passive microwave sensors (SSM/I, AMSR-E or MADRAS) or rainfall satellite products. Copyright © 2012 Royal Meteorological Society

Key Words: satellite-based rain estimation; QPE; conditional bias; geostatistics; rain-gauge; radiometry; West African Monsoon

Received 1 March 2011; Revised 2 March 2012; Accepted 23 March 2012; Published online in Wiley Online Library 29 May 2012

Citation: Kirstetter P-E, Viltard N, Gosset M. 2013. An error model for instantaneous satellite rainfall estimates: evaluation of BRAIN-TMI over West Africa. *Q. J. R. Meteorol. Soc.* **139**: 894–911. DOI:10.1002/qj.1964

1. Introduction

Reliable quantitative information on the spatial distribution of rainfall is essential for hydrologic, meteorological and climatic applications, for assessing risks (flood/drought) or evaluating regional and global atmospheric model simulations. Given their quasi-global coverage, satellite-based quantitative rainfall estimates are becoming widely used for such purposes, especially in the Tropics where the operational ground networks are generally scarce. Converting the satellite (active or passive) measurements into quantitative precipitation estimates is challenging, however. The link between the observations and surface rain rates is indirect. It depends on the spatial heterogeneity of the rain fields, the instrument and the retrieval algorithm. As underlined by the Program to Evaluate High Resolution Precipitation Products (Turk *et al.*, 2008) led by the International Precipitation Working Group (IPWG; see <http://www.isac.cnr.it/~ipwg/>), characterizing the error structure of satellite rainfall products is recognised as a major issue for the usefulness of the estimates (Yang *et al.*, 2006; Sapiano and Arkin, 2009; Wolff and Fisher, 2009; Zeweldi and Gebremichael, 2009). The error needs to be accounted for in climate analysis (Stephens and Kummerow, 2007), over land in hydrological modelling, natural hazards monitoring and assessing water resources (Grimes and Diop, 2003; Lebel *et al.*, 2009).

In this study, we focus primarily on quantitative precipitation estimates (QPE) at the surface, based on low Earth-orbiting passive microwave measurements. Instantaneous estimates from these measurements are usually used in combination with geostationary data to provide gridded precipitation accumulations (Ushio *et al.*, 2006; Ebert, 2007; Bergès *et al.*, 2009). How their uncertainties propagate through such combined products is not totally understood (Chambon *et al.*, 2012). A quantitative and detailed characterisation of these errors is therefore needed. So far this task has been impaired by the difficulty of obtaining a reference rainfall at the retrieval scale of the instantaneous satellite products. In this article we propose an original framework to tackle these issues. The work was developed in the context of Megha-Tropiques preparatory studies, but the methodology could be applied to any rainfall satellite product. Among other instruments, the mission will carry a passive microwave imager (nine channels between 19 and 157 GHz) called MADRAS (Microwave Analysis and Detection of Rain and Atmospheric Structures). The Bayesian Rain retrieval Algorithm Including Neural Network (BRAIN: Viltard *et al.*, 2000, 2006) will be used to estimate instantaneous rain rates from MADRAS measurements. As MADRAS is not available yet, BRAIN has been evaluated using ten years of Tropical Rainfall Measuring Mission (TRMM) Microwave Imager (TMI) data (Kummerow *et al.*, 1998).

A number of studies investigated the quality of instantaneous satellite rainfall estimates in various regions of the world (e.g. Yang *et al.*, 2006; Wolff and Fisher, 2008, 2009), but few have addressed West Africa. Ground validation in this particular region is a difficult task because the operational gauge networks are scarce. High-quality rainfall estimations from satellites are important to compensate operational data network degradation. Satellite products have proven very useful for covering the various scales needed to understand the West African Monsoon

(WAM: Andersen *et al.*, 2002; Redelsperger *et al.*, 2002; Grimes and Diop, 2003; Conway *et al.*, 2009; Roca *et al.*, 2010). In the present study we concentrate on two well-instrumented mesoscale areas in the north of Benin and near Niamey in Niger. Each area is representative of a different eco-climatic zone and rainfall regime: Sahelian for Niger and Sudanese for Benin. We question the ability of space-based rain retrievals to reproduce these differences. These sites belong to the African Monsoon Multidisciplinary Analysis-Couplage Atmosphère Tropicale Cycle Hydrologique (AMMA-CATCH) long-term observing system, in the WAM region (Redelsperger *et al.*, 2006; Lebel *et al.*, 2009, 2010). BRAIN has already been evaluated over oceans (Viltard *et al.*, 2006); this study is the first evaluation of the algorithm over land.

One possible approach is to examine all sources of errors separately and evaluate their cumulative effects (L'ecuyer and Stephens, 2002; Kummerow *et al.*, 2006). However, the underconstrained nature of the rainfall remote sensing impairs the error separation methods, partly because the models used to perform the retrieval are very sensitive to unobserved atmospheric parameters (Yang *et al.*, 2006; Stephens and Kummerow, 2007), particularly over land as discussed in section 2.4. A different approach is proposed here. The problem is addressed by evaluating the satellite QPE overall accuracy with respect to an external, independent reference rainfall. To do so we must evaluate the quality of the so-called reference. One should note that it is not possible to 'validate' the BRAIN-TMI estimates in a strict sense because independent rainfall estimates with no uncertainty do not exist. On the other hand, the available independent measurements do provide a useful reference to help identify possible biases and uncertainties associated with BRAIN-TMI estimates. The problem is addressed by comparing BRAIN-TMI QPEs with reference values derived from ground-based measurements (GV) from densified rain-gauge networks. We use a geostatistical framework to assess the uncertainties of this reference. To evaluate BRAIN-TMI at the regional scale, we use the TRMM Precipitation Radar (PR), which is currently the only active instrument measuring rainfall from a satellite platform conjointly with a radiometer (TMI). PR rainfall estimates are often considered as a reference for TMI-based rainfall estimates (e.g. Yang *et al.*, 2006; Wolff and Fisher, 2008). At the whole WAM region scale, the PR provides an extended but indirect surface rainfall estimation, whereas the rain-gauge networks provide a direct measure of rain rates over a limited area. The PR however suffers from specific errors (section 2.3). Therefore the PR is also compared to the gauges in order to evaluate it as a reference for BRAIN-TMI.

We assess the accuracy of the instantaneous rain products at the original resolution of BRAIN-TMI (i.e. the footprint scale). Comparison of instantaneous products filters out the effects of the temporal sampling error (Wolff and Fisher, 2009). Comparison at the footprint scale avoids bringing in additional uncertainties due to spatial resampling. The BRAIN-TMI, PR and GV rain rates are pixel-matched in both time and space, and spatially averaged at the BRAIN-TMI retrieval scale (12.5 km). Several aspects of errors are revealed and quantified including comparisons of rainfall detectability and rainfall rate distributions, spatial representativeness of error, and separation of systematic biases and random errors. The comparison sample size is an issue for computing robust statistics. To compensate for

the poor temporal sampling of low Earth-orbiting satellites (Lin and Hou, 2008; Wolff and Fisher, 2008, 2009), we use ten years (1998–2007) of satellite overpasses.

The BRAIN-TMI algorithm, the PR data and the reference rainfall used for comparisons are presented in section 2. The representativeness of the comparison datasets is evaluated. Section 3 assesses the ability of BRAIN-TMI and PR estimates to retrieve the reference rainfall features in terms of rainfall occurrence, sensitivity and spatial structure. In addition to BRAIN-TMI performances regarding the rain/no rain detection, the quantitative retrieval is addressed. Section 4 provides an empirical error model of BRAIN-TMI and PR estimates versus reference rainfall. Probability distribution functions (PDFs) of the residuals between reference rainfall and satellite estimates are computed and analysed. We consider the influence of the rainfall intensity, and segregate systematic and random error. Concluding remarks can be found in section 5.

2. Data sources

One of the first challenges is the lack of knowledge about the true average rainfall for the spatial domains considered. The instantaneous satellite rainfall estimate $R(A)$ is compared with a reference rainfall $R_{\text{ref}}(A)$ for a spatial domain A (which may be a satellite mesh, watershed ...). The reference rainfall $R_{\text{ref}}(A)$ is a proxy of the true (and unknown) area-averaged rainfall rate. The reference data $R_{\text{ref}}(A)$ used to evaluate the satellite estimates should spatially match the corresponding true rainfall averaged over the same area A . We consider the residuals between the estimated and reference values to build an error model, with:

$$\varepsilon = (R - R_{\text{ref}}). \quad (1)$$

2.1. Comparison domains

Two rain-gauge networks located in Niger and Benin are used for this study and presented in Table 1 with their gauge distributions shown in Figure 1. Data are provided every 5 minutes and have been collected and quality-controlled continuously since 1998. The distribution of gauges for the network around Niamey was optimised (Lebel and Amani, 1999) to obtain the best possible accuracy over the domain at the rain-event scale (typically a few hours). The number of tipping-bucket gauges was brought up to 54 for the AMMA Enhanced Observing Period in 2006. The Upper Ouémé catchment in Benin was instrumented with 52 tipping-bucket gauges as evenly distributed as possible. On average, both the Ouémé and Niamey networks have a density of about 1 gauge/400 km² (1 gauge/300 km² at their best) over a 1° x 1° area.

The two sites of Benin and Niger differ in terms of rainfall regimes. The convective systems of Niger are considered among the most intense in the world and are usually

associated with strong electric activity and high ice content. The convective systems in Benin are more frequent and offer more diversity. These characteristics certainly explain the differences of annual mean intensity and rain amount between the two sites (Lebel *et al.*, 2009). Figure 2 presents distributions of rain intensities computed from rain-gauges at the BRAIN-TMI spatial scale (see following section). Both the PDF of rain intensity by occurrence (PDF_c) and by volume (PDF_v) are computed as proposed by Wolff and Fisher (2009) and Amitai *et al.* (2009). If the former simply shows the occurrence in percentile of a given interval of intensity, the latter shows the contribution of this rain bin to the total volume. The PDF_c highlights the estimate's sensitivity as a function of rain rate. The PDF_v is computed as a ratio between the sum of the rain rates inside each bin and the total sum of rain rates; it attenuates the influence of light rain rates when comparing PDFs of estimates derived from instruments characterised by different detection thresholds. Both the Benin and Niger PDF_c are unimodal but the mode is about 0.4 mm h⁻¹ for Benin and 0.8 mm h⁻¹ for Niger. The shift of the contribution to the total rain volume towards heavier rain rates in Niger compared to Benin is in agreement with the greater proportion of Mesoscale Convective Systems (MCS) observed over Niger (see following section). In fact, the proportion of heavy rain rates tends to increase when the systems are organised. The comparisons of the lower end of the rainfall intensity spectra have to be interpreted with caution due to the uncertainties in gauge measurement increasing with lower intensities (Ciach, 2003). The features seen in Figure 2 are to be linked to the brightness temperature (T_b) signatures of rain events at 37 GHz and 85 GHz from which BRAIN-TMI infers rain rates at the ground. Figure 3 presents the PDF_c of T_b for the two sites. For all channels considered, the T_b distribution over Niger is shifted towards lower values compared to the Benin PDF_c. The mean T_b at channel 37 GHz is 7 K lower in Niger than in Benin and ~ 15 K lower for either horizontal or vertical polarization at channel 85 GHz. Differences at the warm end of the PDFs when in a non-rainy or lightly rainy situation could be due to the differences in surface emissivity between the two regions. One must notice that the main difference between the two PDFs does not occur at the low end (convection) but roughly in the 230 K range (at 85 GHz), which is usually characteristic of T_b s observed in the stratiform regions. This difference could be due to a difference in ice content, ice density or spatial homogeneity of the ice field. Since the mode of the rain occurrence is slightly higher in Niger, it is likely the ice content that causes the PDF difference in T_b s. This difference in ice content seems then due mostly to the amount of convection rather than its intensity since as previously stated the coldest T_b s are not dramatically colder in Niger.

Table 1. Characteristics of the rain-gauge networks.

Name	Localization		Area (km ²)	No. gauges
Niger – Niamey	13.0° N–14.2° N	1.4° E–3.0° E	25 × 10 ³	54
Sahel area	13.0° N–14.2° N	11.5° W–30° E	5.96 × 10 ⁵	–
Benin – Ouémé	9.0° N–10.0° N	1.5° E–2.8° E	15.4 × 10 ³	52
Northern Savanna area	8.0° N–12.0° N	11.5° W–30° E	2.01 × 10 ⁶	–

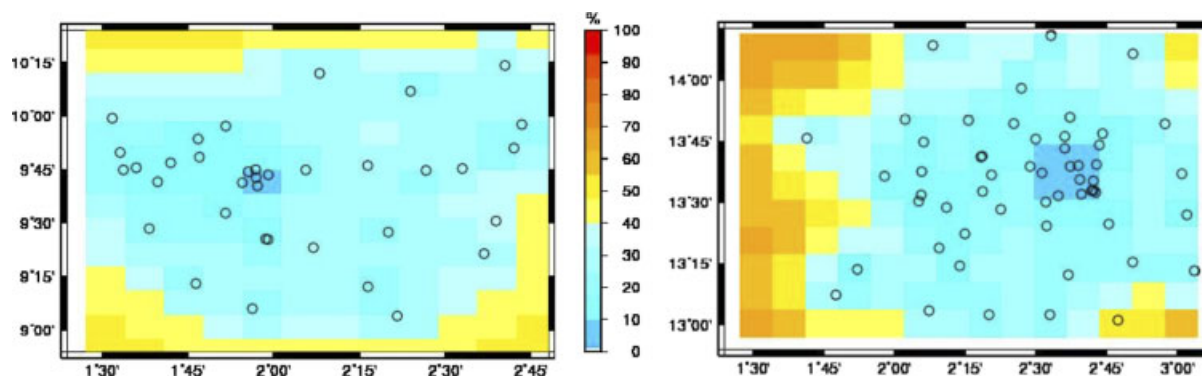


Figure 1. Maps of kriging error in per cent of the rainfall field variance at 5 min time-step and at BRAIN-TMI spatial resolution for the (left) Benin and (right) Niger networks. Circles indicate the effective positions of the rain-gauges. This figure is available in colour online at wileyonlinelibrary.com/journal/qj

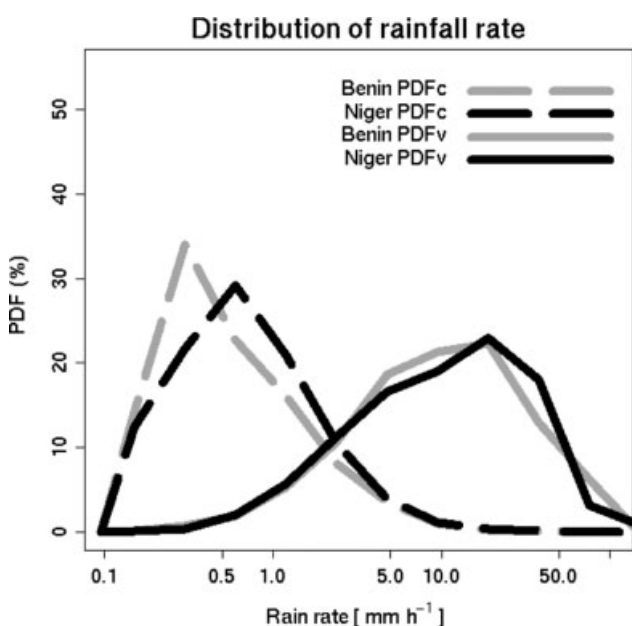


Figure 2. Probability distributions of rain rates for the rain-gauge rainfall kriged at the BRAIN-TMI pixel scale over Benin and Niger. The solid lines represent the distribution by volume $PDF_v = \{R \times PDF(R)\}$ for Benin (grey) and Niger (black) respectively. The dashed lines represent the distribution by occurrence $PDF_c = PDF(R)$ for Benin (grey) and Niger (black) respectively. Note that the x-axis is in log-scale.

2.2. Rain-gauge based rainfall

In the current study, all significant rain events observed coincidentally by TRMM and the rain-gauge networks from 1998 to 2007 over the monsoon period (roughly 1 May to 30 September) were collected, yielding 113 events in Niger and 214 events in Benin. The rain events are defined from the rain-gauge networks using criteria close to D'Amato and Lebel (1998): (i) at least 10 rain-gauges are in working condition; (ii) at least 10% of the rain-gauges record more than 0.5 mm of rain; (iii) at least one station records more than 1 mm; and (iv) the end of the rain event is defined when no rain is recorded at any of the network stations for more than 30 min. The selected events account for 90% of the total rainfall measured over the monsoon period. The measurements closest in time to the TRMM satellite local overpass schedule time are used. For GV, a block-kriging rainfall pixel is computed from gauge measurements

to match each satellite pixel in case of TRMM overpasses (Kirstetter *et al.*, 2010).

Rainfall estimation by gauges is subject to minor instrumental errors due to the direct nature of the measurement, even if uncertainties can be significant for low rain rates (e.g. Ciach and Krajewski, 1999). The limitations of point gauge measurements for a reliable evaluation of area-averaged radar rainfall estimates have already been studied (e.g. Habib *et al.*, 2004). The spatial variability of rainfall at small scales and the large resolution difference between gauge and satellite (as much as 10 orders of magnitude in area) may cause large discrepancies in the statistical sampling properties and add statistical noise in the comparison (Ciach and Krajewski, 1999). The block-kriging linear interpolation estimator (Journel and Huijbregts, 1978) is used to estimate the reference rainfall $R_{ref}(A)$ and the associated sampling error over the BRAIN-TMI footprint A from gauge observations. By weighting the rain-gauges individually, the kriging estimator is unbiased and the estimation variance is minimised (Lebel and Amani, 1999). A detailed description of the block-kriging technique, which provides an unbiased estimate of rainfall and minimises the estimation variance, can be found in Kirstetter *et al.* (2010) and Lebel and Amani (1999). Kriging makes use of a structure function given by a normalised variogram γ (Lebel *et al.*, 1987), which represents the spatial correlation of the rain field.

As a first step, the variogram is used to check if the density of the network is sufficient to capture the structure of the rain field down to the 12.5 km resolution required here. Experimental normalised variograms are computed from the data at the 5 min time step over the period. The following models are fitted in order to describe the structure by a relatively simple function and for the interpolation by kriging:

$$\begin{aligned}\gamma_{Benin}(h) &= 0.57\{1 - \exp(-h/1)\} + 0.56\{1 - \exp(-h/32)\} \\ \gamma_{Niger}(h) &= 0.30\{1 - \exp(-h/1)\} + 0.80\{1 - \exp(-h/28)\}\end{aligned}\quad (2)$$

(with interdistance h in km). Figure 4 shows the experimental variograms as well as the fitted models. Note that up to 30 km, the spatial decorrelation is significantly higher in Benin than in Niger, in agreement with the greater proportion of organised convective systems observed over the latter. The spatial representativeness of the rainfall measurements may be quantified by the mean decorrelation

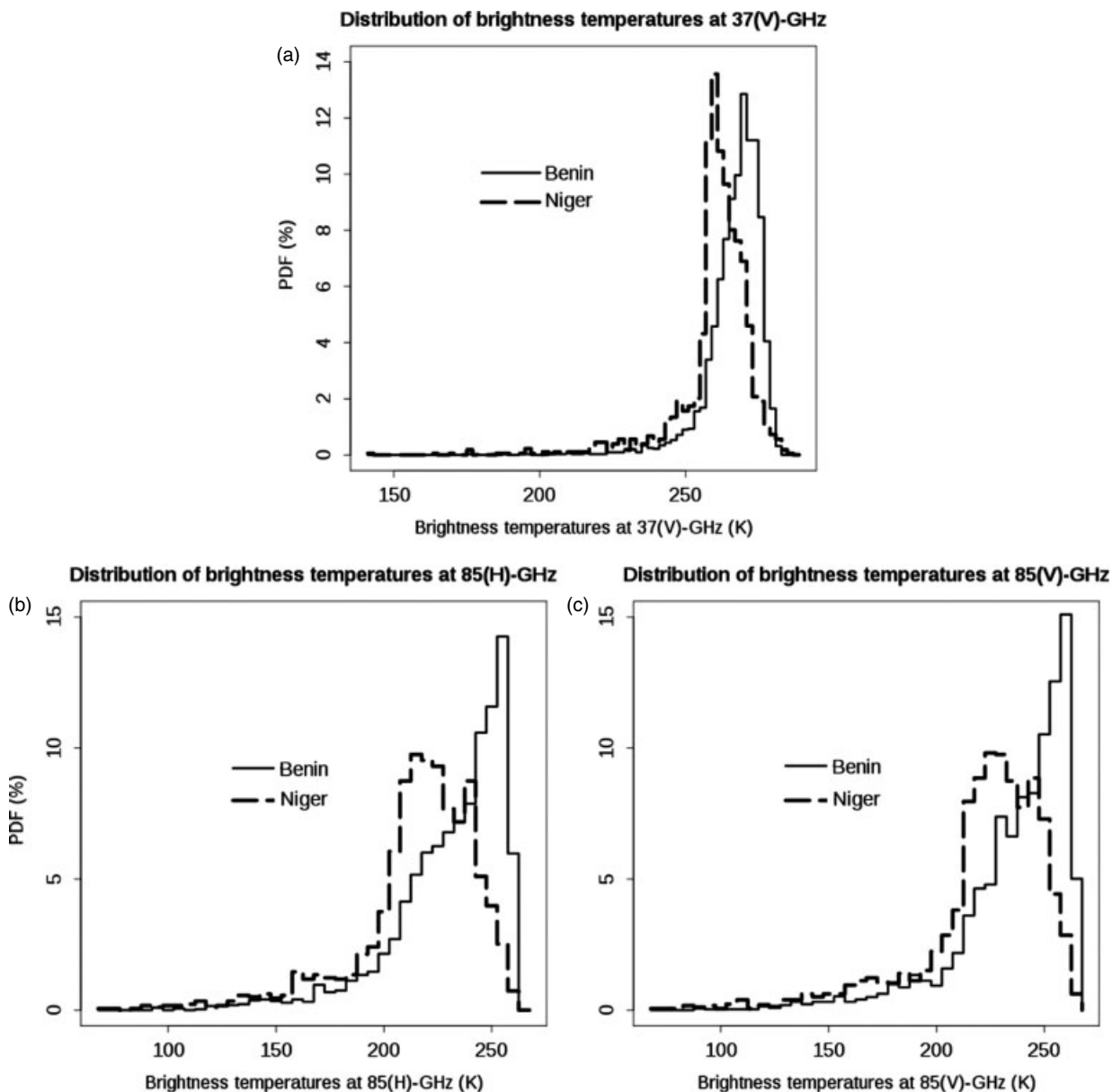


Figure 3. Probability distributions of brightness temperatures over Benin and Niger for rain events only. The solid and dashed lines represent the distributions by occurrence for Benin and Niger respectively for (a) 37 GHz V, (b) 85 GHz H, and (c) 85 GHz V.

distance (the variogram reaches 95% of its maximum). This decorrelation distance is about 70 km for both sites. This means the gauge networks with an average density of 1 gauge every 400 km² can be considered as moderately dense for detecting the variability of rainfall associated with large rainfall systems for 5 min accumulations. Here we need rainfall estimates over BRAIN-TMI pixels. Their quality depends on the decorrelation at small interdistances. The rapid decorrelation of spatial structure at short interdistances suggests that the spatial representativeness of rainfall measurements may be limited, especially in the case of disorganised systems like in Benin. The kriging estimation variance gives a quantitative assessment of the estimation quality. It depends on the variogram and the relative position of the gauges with respect to the estimation domain *A* (Figure 1). As we use a normalised variogram, the estimation variance is expressed in proportion to the field variance (see Kirstetter *et al.* (2010) for more details). Figure 1 shows a map of the Benin and Niger areas with the kriging estimation standard deviation (square root of the

estimation variance) as an indicator of the estimation quality. As expected, the highest quality is found near the densest part of the rain-gauge networks. The estimation degrades for pixels that are further away from the gauge locations. The kriging standard deviation was used as a guideline to select the 'best' pixels in the GV. A two-step selection was applied in order to keep only the pixels with low estimation variance. First, the pixels containing at least one gauge were selected. Second, pixels were further sorted according to their relative error (kriging standard deviation/kriging estimate): they are labelled as 'robust' if the estimated standard deviation is inferior to the estimated value and 'non-robust' otherwise. GV null values are considered as robust. The averaged relative error over the robust GV pixels is 35% while 118% for the whole set in Benin; the values are 25% and 70% for the Niger site. The ratio of the mean error to the standard deviation of the rain-gauge estimates decreases from 13% to 9% in Benin and decreases from 12% to 8% in Niger, when considering only the 'robust' dataset.

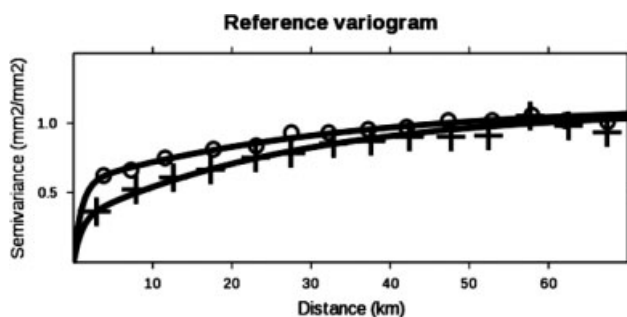


Figure 4. Spatial variograms of rain-gauge data at the 5 min accumulation period for 1998–2007. The empirical variograms are plotted with crosses and circles for Niger and Benin respectively, and the models fitted are represented by the thick black lines.

2.3. Precipitation Radar (PR) based rainfall

The TRMM PR measures the reflectivity profiles at Ku band. In the BRAIN architecture, the PR may be regarded as a ‘calibrator’ of the passive microwave precipitation estimates, while the passive radiometers, already a component of several polar-orbiting observatories, provide more extensive sampling of precipitation events over the globe.

PR observations provide a more direct measurement of the rain rate than TMI. However, some artefacts must be accounted for such as contamination by surface backscatter, attenuation and extinction of signal, bright-band effects and uncertainty of the Z-R relationship (Wolff and Fisher, 2008). In the present study, the surface rain rate at each PR footprint location is a standard TRMM product (2A25 v6) described in Iguchi *et al.* (2000). The scan geometry and sampling rate of the PR lead to footprints spaced approximately 4.3 km cross- and along-track (5.1 after TRMM boost), over a 215 km wide swath centred within the 760 km wide TMI swath; therefore, TMI and PR observations over the PR swath are nearly coincident in time and space, except for a 1 min offset.

The PR pixels falling within 6.25 km of the centre of a TMI pixel are averaged to downgrade the former to the resolution of the BRAIN-TMI product. The minimum theoretically detectable rain rate by the PR is fixed by its sensitivity and is about 17 dBZ, or 0.5 mm h⁻¹, but the spatial averaging at 12.5 km reduces this threshold to roughly 0.3 mm h⁻¹.

2.4. BRAIN TRMM Microwave Imager (TMI) based rainfall

The TMI complements the PR by measuring brightness temperatures at five microwave frequencies: 10.7, 19.4, 21.3, 37.0 and 85.5 GHz. Each frequency is dual polarised (horizontal, H and vertical, V) except for the 21.3 GHz channel, which is only vertically polarised.

The BRAIN-TMI algorithm used here to retrieve surface rainfall from brightness temperatures is described in Viltard *et al.* (2000, 2006). The algorithm relies on a retrieval database made of brightness temperature vectors associated with their corresponding rain rate. Each element of the database is obtained from rain profiles from the PR coupled with a radiative transfer model to generate the corresponding *Tbs*. Since PR provides mostly information on the liquid phase, a base of profiles from the Goddard Cumulus Ensemble is used to set up the ice contents that best match the PR profile following the process detailed in Viltard *et al.* (2000). In the retrieval itself, an observed

brightness temperature vector is compared to each element of the database. BRAIN uses Bayes’s probabilistic theorem to determine the rain-rate profile, *R*, from the *a priori* database given a *Tb* vector:

$$\Pr(R|Tb) = \Pr(R) \Pr(Tb|R) \quad (3)$$

where $\Pr(R)$ is the probability that a certain profile *R* will be observed and $\Pr(Tb|R)$ is the probability of observing the brightness temperature vector *Tb*, given a particular rain-rate profile. The algorithm screens to determine whether or not rain exists and distinguish between rain/no-rain zones before attempting to quantify the rainfall. Viltard *et al.* (2006) showed that the retrieval error is dependent on the rain rate, with maximum errors at the low and high ends of the rain intensities. The retrieval method is optimised to exhibit a low total bias for climatological purposes and thus shows a high standard deviation on a point-to-point comparisons basis.

A complete description of BRAIN is beyond the scope of this article but it is important to note some specific issues for the rainfall retrieval over land. Over land only the scattering channels (namely 85 GHz and 37 GHz) can be used because of the radiometrically warm land surface. As the brightness temperature at these frequencies is mostly sensitive to the scattering processes in the higher regions of the cloud (Wilheit *et al.*, 2003), the available information for the retrieval is not directly related to the surface rainfall. Hence there are particular needs for a detailed assessment of BRAIN-TMI performances especially regarding the rain/no-rain mask and the quantitative retrieval.

2.5. Comparison samples and domains

Several factors including rainfall intermittency, the discrete temporal sampling of TRMM, differences of swath between TMI and PR and the selection of limited number of ‘robust’ GV pixels (see above) reduce the number of comparison samples over the ten-year period. Table 2 provides the number of these samples for the different sensors, inclusive and exclusive of non-rainy pixels (0 mm h⁻¹). The sample sizes for GV/BRAIN-TMI comparison (Table 1) are primarily limited by the overpass frequency of TRMM and the number of rain events; as rain events are more frequent in Benin than in Niger, the number of samples is larger in this area.

In order to assess the representativeness of the two AMMA-CATCH networks, the same statistics were also computed over two extended regions similar to those described in Geerts and Dejene (2005) and summarized in Table 1. The Benin GV site is included in their northern Savanna region and the Niger GV site is included in their Sahel region. These climatic regions are each characterized by distinct and rather homogenous rainfall regimes (Nicholson *et al.*, 2000, 2003; Leroux, 2001; Adeyama and Nakamura, 2003). Figure 5 shows quantile–quantile plots between (i) the BRAIN-TMI and PR datasets for the two extended climatic regions (*x*-axis), and (ii) the subset of satellite pixels that match the GV for the two validation sites. Table 3 provides values of the conditional mean and standard deviation. The ‘GV-resampled’ BRAIN-TMI rainfall distribution (Figure 5(a) and (c)) does not show a clear deviation from the 1:1 line compared to the regional distribution. The Benin (Niger) mean estimate is within

Table 2. Comparison samples for different couples of sensors.

	Benin		Niger	
	Including non-rainy (0 mm h ⁻¹)	Rainy only	Including non-rainy (0 mm h ⁻¹)	Rainy only
BRAIN-TMI (GV domain)	9123	2286	6596	1524
BRAIN-TMI (climatic regions)	133 027	7655	43 201	2287
PR (GV domain)	1498	555	1290	584
PR (climatic regions)	133 027	12 662	43 201	3769

The samples are computed for rain events as defined by the gauge networks over the GV domains. In addition, all comparison pairs of BRAIN-TMI and PR are included over the two climatic regions.

Table 3. Conditional mean and standard deviation of comparison samples for the two satellite-based estimates.

	Benin		Niger	
	Mean (mm h ⁻¹)	St. dev. (mm h ⁻¹)	Mean (mm h ⁻¹)	St. dev. (mm h ⁻¹)
BRAIN-TMI (GV domain)	4.92	4.40	7.30	6.39
BRAIN-TMI (climatic regions)	4.46	4.69	7.03	6.00
PR (GV domain)	3.77	4.50	3.43	3.56
PR (climatic regions)	3.24	3.86	3.76	4.07

The samples are computed for rain events as defined by the gauge networks over the GV domains. In addition, all comparison pairs of BRAIN-TMI and PR are included over the so-called climatic regions.

10% (6%) of the Northern Savanna (Sahel). The PR shows slight departures from the 1:1 line on PDF_c comparison and greater quantitative differences (the mean estimates over GV sites present differences greater than 15% compared to the two extended climatic regions). This suggests that the sampling of BRAIN-TMI over both sites for the ten-year period is quite representative of the corresponding climatic distribution of rainfall. The larger departures of the PR estimates are likely due to the more limited number of samples. We need to consider the climatological sample when comparing PR to other sensors.

To assess the impact of the limited temporal sampling of TRMM, we compared the satellite overpass-resampled GV dataset with the entire time series. Figure 6 provides for both sites quantile–quantile plots between (i) the whole GV dataset (*x*-axis), and (ii) the subset of pixels that match a TMI and a PR overpass respectively. Table 4 provides the corresponding conditional mean and standard deviation. For the TMI overpasses over both GV sites the latter shows a slight underestimation within 10% of the reference values. The underestimation is significantly greater for the PR sampling (e.g. greater than 10% in Benin and up to 32% in Niger for the mean). These results suggest that the TMI samplings over the AMMA-CATCH sites for the 10-year period are representative of the corresponding local climatic distribution of rainfall. The limited PR swath is a likely explanation for the undersampling of rainfall events over the two GV sites (Table 2). This affects the detection of higher and less frequent rainfall intensities. The ‘PR-resampled’ distribution of rainfall is consistently shifted towards lower

values than the ‘BRAIN-TMI resampled’ and the whole GV sets.

3. Rainfall data analysis

This section analyses the ability of PR and BRAIN-TMI rain retrievals to reproduce the rainfall variability derived from the rain-gauge data. First, contingency tables show the links between BRAIN-TMI and the PR rainfall detection and the GV reliability. The PDFs of rainfall estimates provide in-depth information on the sensors’ sensitivity to rainfall regime differences. The spatial structures of the rainfall fields are also compared.

3.1. Contingency tables

Table 5 shows the contingency tables for PR relative to GV with percentile of Hits (*H*, both GV and PR detect rain), Misses (*M*, PR does not detect rain while GV does), False alarms (*F*, PR detects rain while GV does not), and Correct rejections (*C*, both GV and PR do not detect rain) over both sites. The GV data are separated into three sub-samples: the non-robust set, see section 2.2, the robust GV set and the ‘whole’ GV set. GV null values are considered as robust. All coincident and collocated PR values are considered and sorted according to the GV samples. Table 6 provides the mean rainfall values according to the same contingency tables, with PR on the left-hand side of the ‘/’ sign and the GV on the right-hand side. The false detections (*M* + *F*) of

Table 4. Conditional mean and standard deviation of GV.

	Benin		Niger	
	Mean (mm h ⁻¹)	St. dev. (mm h ⁻¹)	Mean (mm h ⁻¹)	St. dev. (mm h ⁻¹)
Whole GV set	4.09	7.04	4.49	7.67
BRAIN-TMI sampled GV	4.00	6.45	4.25	7.01
PR sampled GV	3.63	5.57	3.03	4.21

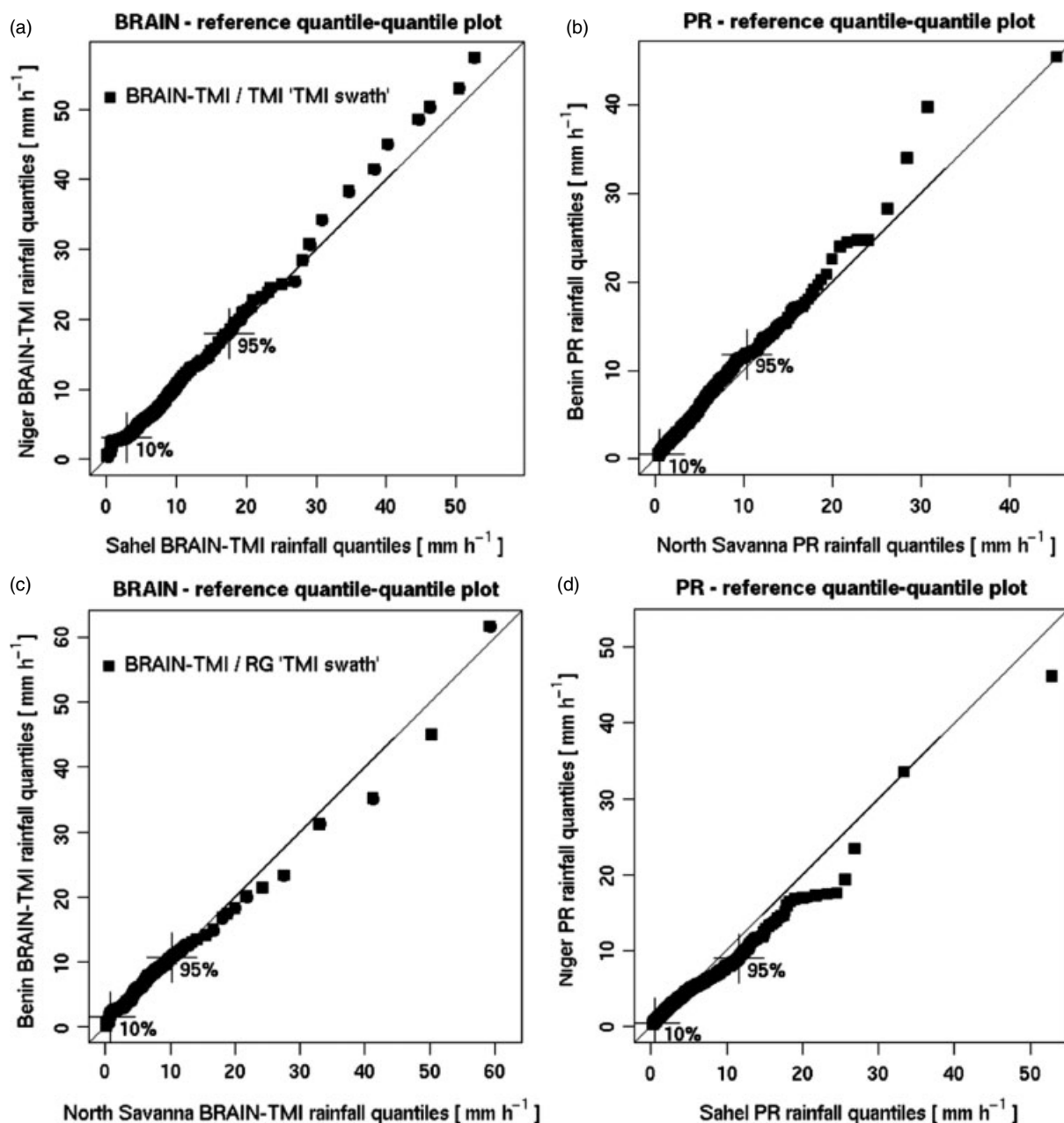


Figure 5. Quantile–quantile plots of the rainfall distribution for the GV sites (y -axis) and the regional area (x -axis) over (a)–(b) Niger/Sahel and (c)–(d) Benin/Northern Savanna, for (left) BRAIN-TMI and (right) PR. ‘RG’ denotes rain-gauge. The positions of the 10 and 95 percentiles are showed for each distribution.

PR are mainly associated with the non-robust GV data: 72% in Benin and 61% in Niger. Only 16% in Benin and 14% in Niger are improperly classified when using the ‘robust’ GV dataset. The Misses (M) are the main contributors to the false detection population (i.e. 95% in Benin and 85% in Niger for the ‘whole’ dataset). These Misses of PR are coincident with low GV values (see Table 6: 0.1 mm h^{-1} for the non-robust set for both Benin and Niger). By comparison, the correct detections ($H + C$) of PR are mainly associated with the robust GV set (more than 80% for both sites). For the same robust GV set, the Hits of PR are coincident with the higher GV values with mean rainfall rates equal to 4.2 mm h^{-1} in Benin and 3.1 mm h^{-1} in Niger. One should note for both sites that (i) the mean PR (F) values are significantly lower than the mean PR (H) values, and (ii) the mean GV (M) values are significantly lower than the mean GV (H) values. Finally both mean GV and PR values

are higher for the robust GV set than for the non-robust GV set. The discarded rain volumes by Misses of PR represent 9% of the GV rainfall volume in Benin and 6% in Niger. False alarms represent 3% and 2% of the PR rainfall volume in Benin and Niger, respectively. To estimate the minimum value detectable by the PR, we use the ‘whole’ GV dataset (since the ‘robust’ dataset is defined as points for which the standard deviation is lower than the GV value itself, it is not very representative of the light rain intensities). Considering that 80% of the ‘whole’ GV rain rates that are not detected by the PR in Benin and Niger are lower than 0.3 mm h^{-1} , the sensitivity of the PR at the BRAIN-TMI resolution is confirmed to be close to this value. Despite the limited number of direct comparisons between GV and PR, the similarity of our results in Benin and Niger is an indication of their consistency. The (M) are probably associated with high intermittency and/or the ‘rain/no rain’ limits of rain

fields. These features are not robustly dealt with by the kriging technique because the spatial structure is unclear at the edges (as discussed in section 2.2 and Figure 4). The PR probably misses them because the rain rates are close to the detection threshold. They are consistently more frequent in Benin. This suggests that the PR can indeed capture the main rain regions but loses the weaker echoes (Schumacher and Houze, 2000), probably due to its sensitivity. The discarded rainfall volumes remain limited and need to be compared to BRAIN-TMI's in order to evaluate the PR as a reference for BRAIN-TMI.

Table 7 shows the contingency tables for BRAIN-TMI relative to the GV datasets. Table 8 provides the corresponding mean rainfall values. The same comments as for PR can be made for TMI. Misses (M) contribute totally to the false detection. A similar result arises when using the PR as a reference over the climatic regions. This suggests that BRAIN-TMI, as PR, misses the lightest intensities. Based on Table 8, 0.6 mm h^{-1} appears to be the sensitivity threshold for BRAIN-TMI. The false detections are more significant with 'robust' GV than for PR (27% in Benin and 32% in Niger – Table 7). It should be noted that the GV mean values (robust case) are 33% and 116% higher in Benin and Niger respectively in Table 8 (TMI) than in Table 6 (PR). A similar feature can be seen for the Misses. It seems that the BRAIN-TMI retrieval is performed over the 'rainiest' zones only. This effect is probably due to the fact that BRAIN-TMI retrieves rain only when a clear scattering signature is detected in the T_b s. This effect is expected to be particularly sensitive in the no-rain to light-rain transition regions of the rain systems and also for all the events with no developed ice phase (as in the case of warm rains that are more frequent in Benin). In order to assess the discarded rain volume by Misses, Table 9 provides the percentile of Hits and Misses of BRAIN-TMI relative to 'robust' GV over the two GV sites and relative to PR over the two climatic regions in percentages of the total rain volume for GV and PR respectively. The False Alarms are negligible. Hits and Misses are similar over the two sites and with the two references. The (H) range from 40% to 48%, the (M) from 52% to 60%, showing that BRAIN-TMI detects no rain (and provide no retrieval) in more than half of the rain fields. The Hits and Misses relative to PR are very consistent in the Sahel and Northern Savanna regions. The missed rain volumes range from 22% to 34%.

The conclusion of this comparison between PR, GV and BRAIN-TMI would be that the latter misses at least 20% of the rain volume due to its rain/no-rain mask. The performances of PR are generally better than BRAIN-TMI and the discarded rainfall volumes by Misses of PR are limited compared to BRAIN-TMI. Provided that the results from this study are representative enough, PR can be used as a reference to evaluate the BRAIN-TMI mask over land.

3.2. Probability distributions by occurrence and rain volume

Hereafter, the TMI and PR rain estimates are the conditional ones (positive rainfall) coincident and collocated with the non-zero GV estimates. For the PR, the rain statistics are computed for the climatological regions (Savanna and Sahel) which are the only ones to be representative enough (see section 2.4).

PDF_c and PDF_v for PR versus GV on the Benin and Niger sites are shown in Figure 7. The rain rates from PR exhibit similar PDF_c in Benin and Niger. Compared to

GV's PDF_c, PR tends to overestimate the lighter rain rates ($\sim 0.3\text{--}0.7 \text{ mm h}^{-1}$). PR demonstrates poor detection of the lightest rain rates (below $\sim 0.3 \text{ mm h}^{-1}$) on both sites, as expected from the previous section. The PR and GV PDF_c presents similar features for rain rates $> \sim 1 \text{ mm h}^{-1}$. Despite the low occurrence of relatively high rain rates ($>10 \text{ mm h}^{-1}$), their contribution to the total rainfall volume is significant (greater than 60%). The mode of PDF_v for PR is shifted toward lower rain rates ($\sim 10 \text{ mm h}^{-1}$) compared to the GV mode ($\sim 18 \text{ mm h}^{-1}$), in agreement with the results found in Amitai *et al.* (2006, 2009). This is attributed to high rainfall rates ($>10 \text{ mm h}^{-1}$), which may be underestimated by PR because of insufficient correction due to attenuation losses as suggested by Wolff and Fisher (2008) for the 2A25 version 6. From Figure 7(c), this feature is slightly but consistently more significant in Niger than in Benin, higher rainfall being proportionately more frequent in the former. These features should be taken into account when considering the PR as a reference for BRAIN-TMI.

Figure 8 is similar to Figure 7 except for BRAIN-TMI. BRAIN-TMI generally does not detect the lightest rain rates (below 1.5 mm h^{-1}) very well. This trend has already been mentioned in Wolff and Fisher (2009) for TMI-based estimates over Melbourne, Florida. Again, this is likely due to the difficulty in separating weakly rainy from non-rainy zones solely based on the brightness temperatures at 37 and 85 GHz. (The situation is slightly more favourable in Niger where the GV PDF_c is shifted towards heavier rain rates when compared to Benin.) BRAIN-TMI estimates show a tendency to overestimate the occurrences of rain rates in the range $2\text{--}20 \text{ mm h}^{-1}$. The mode of the BRAIN-TMI PDF_c is therefore shifted from $0.5\text{--}1.5 \text{ mm h}^{-1}$ (GV) to around 4.5 mm h^{-1} , and consistently greater in Niger than in Benin. As a consequence, both PDF_v for BRAIN-TMI show their highest peak around 4 mm h^{-1} ($\sim 50\%$ of the total amount). As for GV, BRAIN-TMI PDF_v in Niger is shifted towards heavier rain rates than in Benin.

Not surprisingly, the PDFs of PR estimates over land are significantly better than BRAIN-TMI. The PR distributions mostly match the GV distributions and show increased skill in detecting the lighter rain rates. PR could be used as a reference to evaluate the BRAIN-TMI PDFs over land, but we need to keep in mind that PR like BRAIN-TMI underestimates the heaviest rain rates. BRAIN-TMI detects more clearly than PR the differences in rainfall regime between Benin and Niger.

3.3. Spatial structure of the estimated rainfall fields

For hydrological applications, the total amount of water over a basin as well as its location and spatial correlation within the catchment might be important. This is relevant for assessing the ability of space-based estimates to retrieve the spatial structure of rainfall fields as seen by GV.

An appropriate model is fitted to the empirical normalised variograms. Among the set of classical models, the spherical model was found most suitable. The difference of spatial resolution of the data (points versus 12.5 km domains) needed for a different model fitting from the double

Table 5. Contingency table for PR over Benin and Niger areas.

	Benin			Niger		
	Whole set GV 3080 pts	Robust GV 1 1498 pts	Non-robust GV 1582 pts	Whole set GV 2164 pts	Robust GV 1290 pts	Non-robust GV 874 pts
Hits (<i>H</i>)	35%	44%	28%	46%	51%	39%
Misses (<i>M</i>)	43%	11%	72%	28%	5%	61%
False Alarms (<i>F</i>)	2%	5%	–	5%	9%	–
Correct rejection (<i>C</i>)	20%	40%	–	21%	35%	–

The results are provided for robust/non-robust GV data according to a criterion based on the relative error: (kriging standard deviation/kriging estimate) > 1.

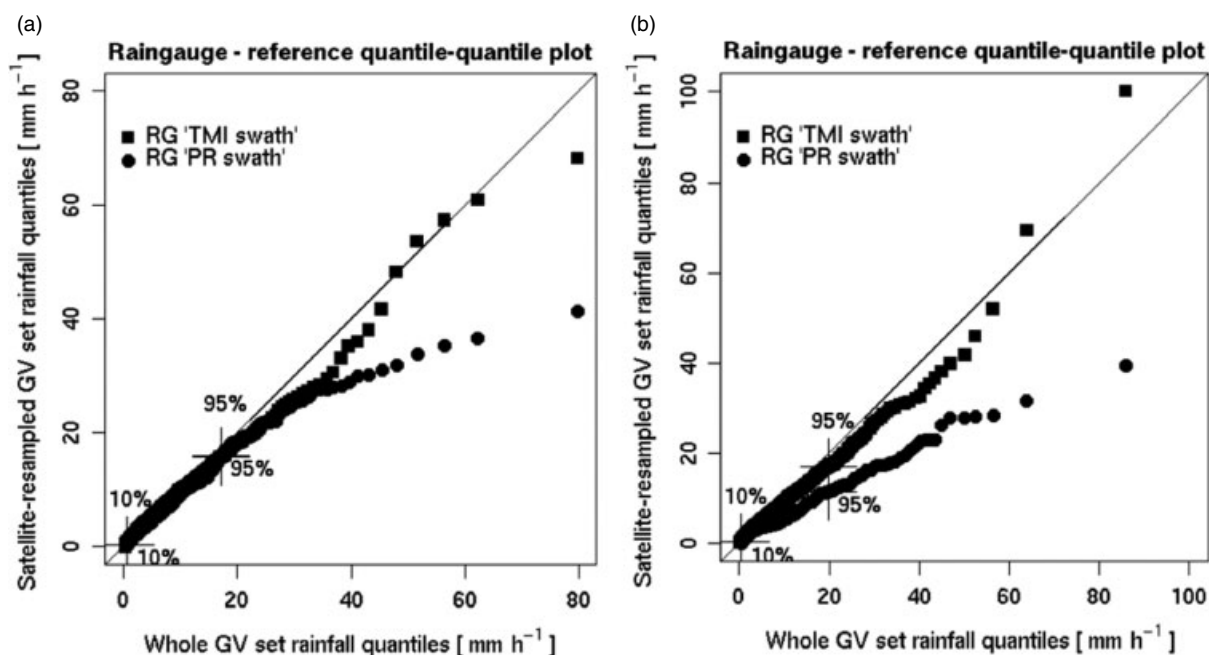


Figure 6. Quantile–quantile plots for GV ‘satellite sampled’ and ‘continuously temporal’ rainfall distribution comparison over (a) Benin and (b) Niger. The positions of the 10 and 95 percentiles are shown for each distribution.

exponential proposed for the GV data in Eq. (2) is used:

$$\gamma(h) = C_0 + (C - C_0) \left(\frac{3h}{2d} - \frac{1}{2} \left(\frac{h}{d} \right)^3 \right) \text{ for } 0 < h < d \tag{4}$$

$$\gamma(h) = C \text{ for } h > d \tag{5}$$

where the three parameters are the nugget (C_0), the sill (C) and the variogram range (d). The spherical model is suitable when the empirical variogram effectively presents a sill, theoretically equal to the field variance, beyond the range (d), which corresponds to the mean decorrelation

distance of the estimates. The nugget parameter can be used to describe a possible discontinuity of the variogram at the origin which may be due to (i) the process variability at scales poorly resolved by the observation system, and/or (ii) measurement errors. In the following, these parameters are used to characterise the structure of rainfall. Normalised variograms of GV, PR and BRAIN-TMI estimates are displayed in Figure 9. Table 10 summarises the parameters of these variograms.

The nugget values are very distinct depending on the sensor. This is limited for GV (around 10% of the sill) and more significant for TMI (three times greater). The smaller GV nugget is an indication of a better sampling for the reference rainfall, as discussed in detail in section

Table 6. Mean rainfall values associated to the contingency table for PR/GV over Benin and Niger areas.

	Benin			Niger		
	Whole set GV (mm h ⁻¹)3080 pts	Robust GV (mm h ⁻¹)1498 pts	Non-robust GV (mm h ⁻¹)1582 pts	Whole set GV (mm h ⁻¹)2164 pts	Robust GV (mm h ⁻¹)1290 pts	Non-robust GV (mm h ⁻¹)874 pts
Hits (<i>H</i>)	2.4/2.6	3.2/4.2	1.2/0.2	2.2/2.1	3.1/3.1	0.7/0.2
Misses (<i>M</i>)	0.0/0.3	0.0/1.6	0.0/0.1	0.0/0.3	0.0/1.6	0.0/0.1
False alarms (<i>F</i>)	0.9/0.0	0.9/0.0	–	0.5/0.0	0.5/0.0	–
Correct rejection (<i>C</i>)	0.0/0.0	0.0/0.0	–	0.0/0.0	0.0/0.0	–

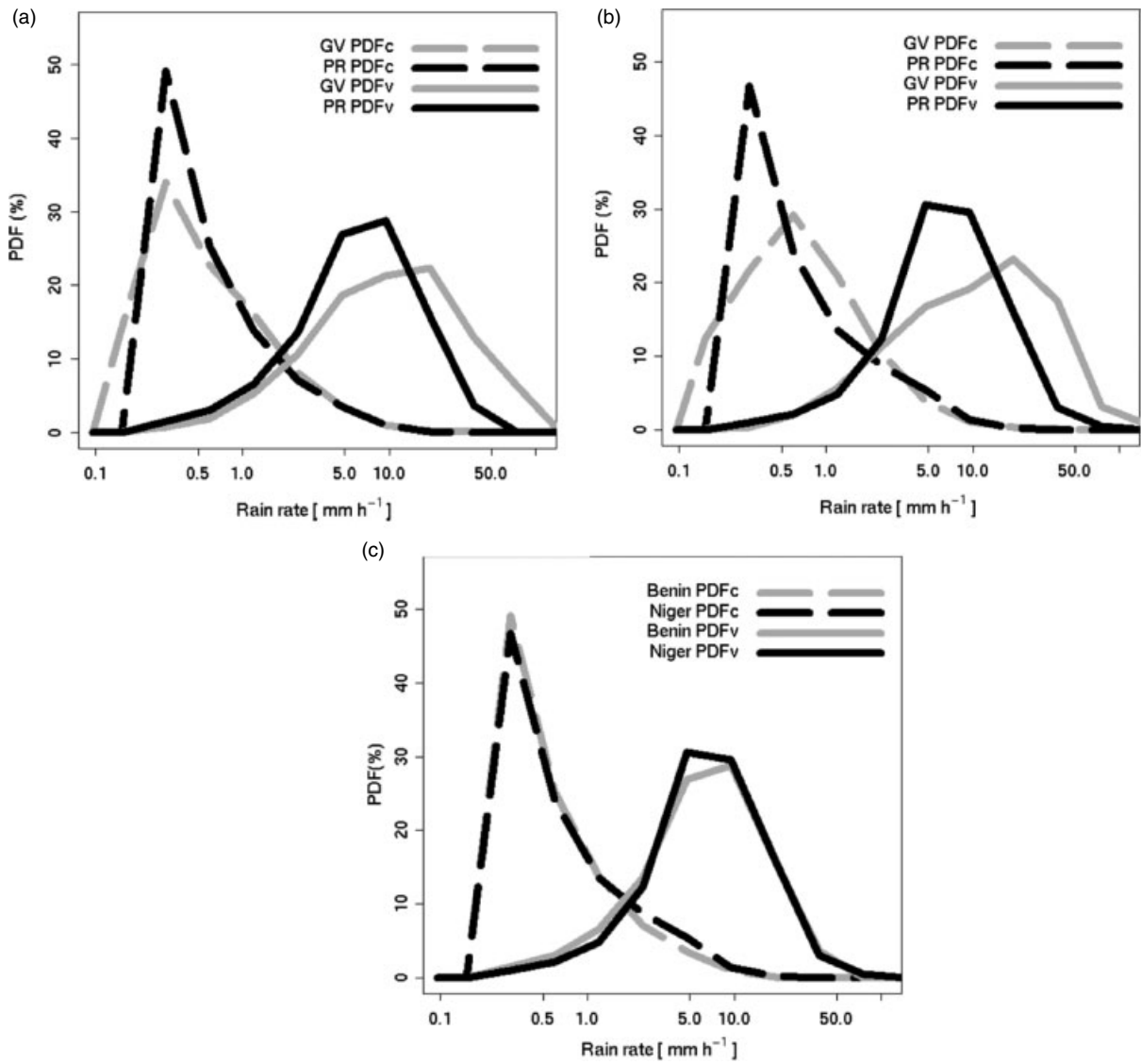


Figure 7. Probability distributions of rain rates for the GV and the PR rainfall over (a) Benin/Northern Savanna and (b) Niger/Sahel. The solid and dashed-dotted lines represent the distribution by volume PDF_v, and the distribution by occurrence PDF_c respectively, while the grey and black lines represent the distributions for GV and PR respectively. (c) Probability distributions of rain rates for the PR rainfall over Northern Savanna (grey) and Sahel (black). Note that the x-axis is in log-scale.

Table 7. Same as Table 5 but for BRAIN-TMI.

	Benin			Niger		
	Whole set GV 17942 pts	Robust GV 9123 pts	Non-robust GV 8819 pts	Whole set GV GV 11601 pts	Robust GV 6596 pts	Non-robust GV 5005 pts
Hits (<i>H</i>)	17%	25%	9%	15%	23%	4%
Misses (<i>M</i>)	58%	27%	91%	60%	32%	94%
False alarms (<i>F</i>)	0%	1%	–	0%	0%	–
Correct rejection (<i>C</i>)	25%	47%	–	25%	45%	–

Table 8. Same as Table 6 but for BRAIN-TMI.

	Benin			Niger		
	Whole set GV (mm h ⁻¹)17942 pts	Robust GV (mm h ⁻¹)9123 pts	Non-robust GV (mm h ⁻¹)8819 pts	whole set GV (mm h ⁻¹)11601 pts	Robust GV (mm h ⁻¹)6596 pts	Non-robust GV (mm h ⁻¹)5005 pts
Hits (<i>H</i>)	4.5/4.2	4.9/5.6	3.3/0.3	7/5.9	7.3/6.7	5.4/0.4
Misses (<i>M</i>)	0/0.7	0/2.5	0/0.1	0/0.8	0/2.5	0/0.1
False alarms (<i>F</i>)	–	2.8/0	–	–	–	–
Correct rejection (<i>C</i>)	0/0	0/0	–	0/0	0/0	–

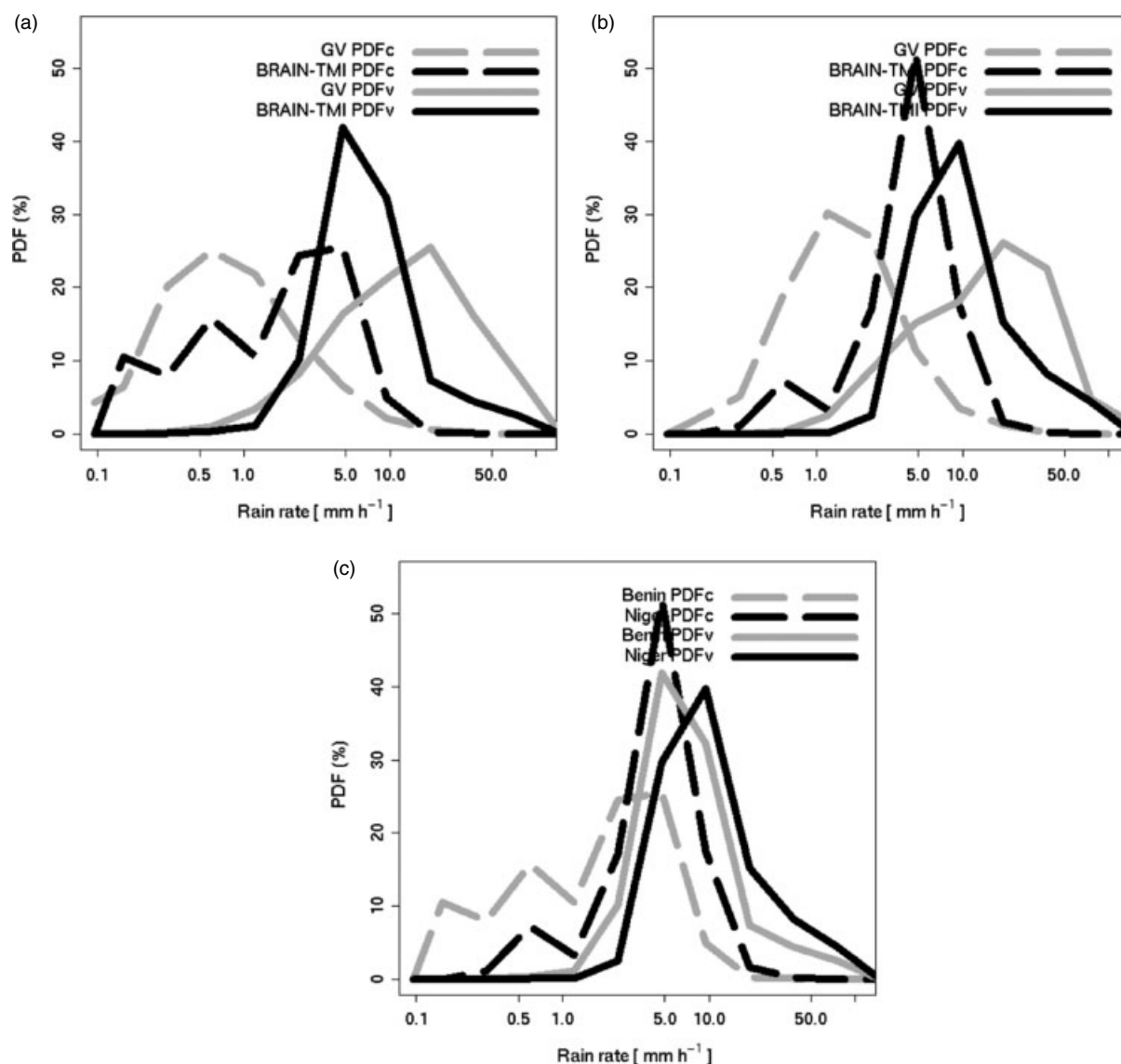


Figure 8. Same as Figure 7 but for BRAIN-TMI.

2.2. The decorrelation of the BRAIN-TMI spatial structure at short interdistances suggests that the independently adjacent retrievals by BRAIN are affected by the noise of the brightness temperatures at the 85 GHz channel. As the BRAIN-TMI rain mask (where BRAIN-TMI performs retrieval) is essentially restricted to the more intense rain rates (see section 3.1), we applied the mask to PR data to compare the variograms within and outside the mask. The variogram computed with the whole PR dataset presents a large nugget (around 60% of the sill) that could be explained by the rain intermittency, contamination by surface backscatter, attenuation of the signal, or inaccuracy of the Z-R relationship. Within the BRAIN-TMI rain mask, the nugget significantly decreases,

getting closer to the BRAIN-TMI one in both Northern Savanna and Sahel. This indicates that the rain fields outside the BRAIN-TMI rain mask are significantly more disorganised, intermittent and noisy than inside, which is consistent with the concept of rain areas that are not detected by TMI and might be only partially detected by PR.

The variogram ranges of BRAIN-TMI and PR are quite similar to GV's (around 30 km) although the former presents a slightly greater range (about 5 km) than GV's. This feature can be related to the fact that BRAIN-TMI rainfall distribution is narrower than GV's, which is consistent with a smoothing of the rain fields and an increase of the decorrelation distance of the estimates. The range of the

Table 9. Hits and Misses of BRAIN-TMI relative to GV and PR rainfall with discarded rain volume by BRAIN-TMI due to Misses relative to GV and PR.

	Benin/Northern Savanna		Niger/Sahel	
	Robust GV (9123 points)	PR (133 027 points)	Robust GV (6596 points)	PR (43 201 points)
Hits (<i>H</i>)	48%	40%	42%	41%
Misses (<i>M</i>)	52%	60%	58%	59%
Discarded rain volume	32%	29%	34%	22%

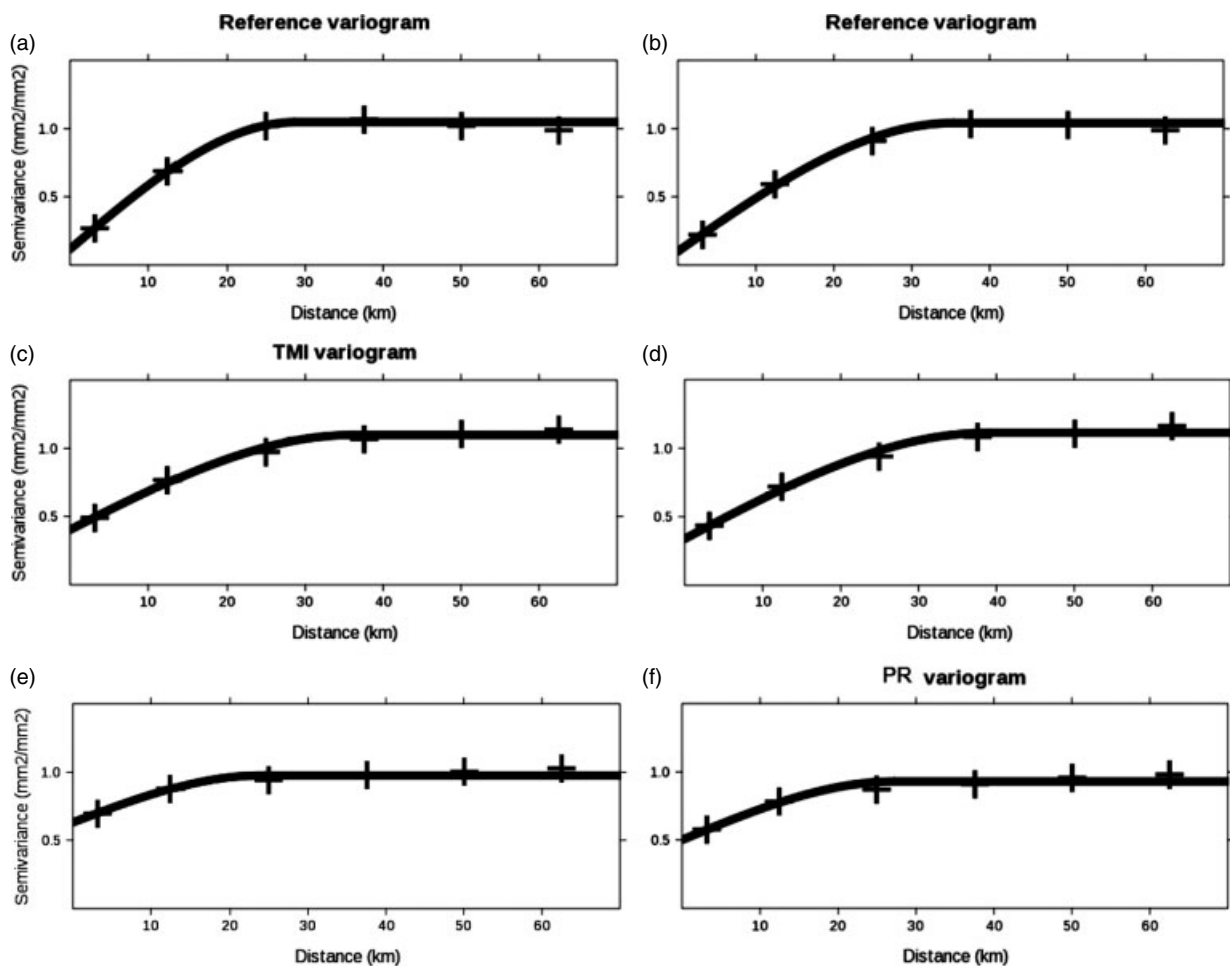


Figure 9. Spatial variograms for (a)–(b) GV, (c)–(d) BRAIN-TMI and (e)–(f) PR, over (left) Niger/Sahel and (right) Benin/Northern Savanna for the 1998–2007 period. The empirical variograms are plotted with crosses, and the models fitted are represented by the thick black lines.

Table 10. Parameters of the normalised variograms (spherical model) for GV, BRAIN-TMI and PR. The nugget is expressed as a percentage of the normalised sill. The values for PR variograms restricted to the BRAIN-TMI mask are indicated (brackets).

	Benin/Northern Savanna		Niger/Sahel	
	Nugget (% sill)	Range (km)	Nugget (% sill)	Range (km)
GV	11	29	9	35
BRAIN-TMI	37	36	31	39
PR (PR/BRAIN-TMI)	65 (43)	24 (36)	54 (34)	27 (42)

whole PR dataset is slightly smaller than GV, indicating less spatial organisation of the PR rain fields; the PR range consistently increases when it is computed using pixels belonging to the BRAIN-TMI rain mask only.

All sensors have a larger nugget over Benin than Niger (+22% for GV, +20% for BRAIN-TMI and +20% for PR). This is consistent with the higher semi-variance values at short interdistance found for the Benin rain-gauge variogram compared to Niger (Figure 4). Furthermore, the range of the variograms tends to increase from Benin to Niger for all sensors (+6 km for GV, +3 km for BRAIN-TMI and +3 km for PR). These consistent findings could be related to the increased proportion of disorganised rainfall structures associated with localised convection in Benin relative to Niger (Depraetere *et al.*, 2009; Vischel *et al.*, 2011). This could lead to enhanced beam filling and intermittency effects on BRAIN-TMI in Benin, resulting in less-spatially correlated estimated rain fields.

4. Quantitative error modelling

In this section, the performances of PR and BRAIN-TMI estimates relative to GV are evaluated by means of correlation and biases. In the rest of the document, the comparisons between the satellite-based and GV estimates are assessed on a point-to-point basis. A rainy pixel is included in the statistics if both PR or BRAIN-TMI and the GV are raining pairs, in order to emphasise the PR and BRAIN-TMI ability to quantify precipitation. This choice is particularly significant for BRAIN-TMI estimates since retrievals are performed over the most restricted rainy zones.

4.1. Correlations and biases

Table 11 provides a summary of the performances of both PR and BRAIN-TMI, compared to GV, based on the correlation coefficient and the mean relative error

(MRE). The latter is expressed in percentage and defined as $MRE = (\text{Sat_mean} - \text{GV_mean})/\text{GV_mean}$. For PR/GV comparisons that are outlined in section 2.4, the comparison sample may not be significant enough to provide robust statistics due to the PR limited swath. Additional MRE values are therefore computed with the whole GV dataset (not necessarily matching a PR overpass) and the PR data over the climatological regions as an indication of PR biases.

The sensors' sensitivity and the representativeness of the comparison samples explain the mean and standard deviation values. As expected, the Niger area shows higher mean rain rates than the Benin area: 10% higher for the whole GV dataset, 20% higher for the 'BRAIN-TMI resampled' GV set, 16% higher for the climatological PR sample and 50% higher for BRAIN-TMI.

The different trend observed for the point-to-point comparison set between PR and GV is attributed to its limited representativeness (section 2.4). Yet there is some consistency as both PR and GV (i) show lower means in Niger than in Benin, (ii) show higher means with this specific dataset than with the other samples in Benin, and (iii) show lower means with this specific dataset than with the other samples in Niger.

BRAIN-TMI shows generally higher mean and standard deviation values than PR and lower standard deviation than GV in coherence with the PDF features presented in section 3.2. The PR estimate over the two climatological regions is lower by about 21% when compared to the Benin GV mean and 16% when compared to the Niger GV mean. Although the climatological regions are larger than their respective GV regions, this could be due to the significant underestimation of the higher rain rates in the 2A25-v6 products. When considering the pixels that are rainy for BRAIN-TMI, the latter shows low biases relative to GV (below 12%). Note that BRAIN-TMI retrieval presents a higher gradient in latitude than GV given the underestimation in Benin (−12%) and the overestimation in Niger (+9%). BRAIN-TMI retrievals are highly dependent on rainfall climatology through the Tb distributions at 37/85 GHz channels. These distributions indicate more frequent deep convection (colder Tbs) in Niger and shallower convection and possibly warm rain in Benin (Figure 2). Overestimation of low to moderate rain rates as seen in section 3.2 could explain the observed positive bias in Niger. Non-uniform beam-filling effects linked to disorganised rainfall structures associated with local convection in Benin could explain the observed negative bias in Benin. Finally, warm rain microphysics (increasing water content near the ground: Xu *et al.*, 2008) could also contribute to a negative bias in Benin given that these formation processes are more prevalent than in Niger.

The correlation coefficients between satellite-based and GV estimates are always low (below 0.5). The differences can be attributed to sample volume discrepancies, timing and navigation mismatches and the uncertainties in the respective rainfall estimates. The significantly greater nugget in the PR variogram than in the GV variogram is also an indication of the greater level of noise in the PR rain field spatial structure, which may limit the correlation between the two estimates. Similarly, as stated by Viltard *et al.* (2006), the BRAIN-TMI algorithm relies on Bayes' theorem and is designed to optimise the overall bias, which increases the variance.

4.2. Error model: conditional distribution of the residuals (satellite QPE - GV)

The uncertainties associated with satellite estimates of rainfall include systematic as well as random errors from several sources (Yang *et al.*, 2006). There is a fundamental issue in segregating the proportion of the scatter due to purely random error, and the proportion due to rain rate-dependent conditional biases of both BRAIN-TMI and PR that may be either positive or negative, producing additional scatter. As the BRAIN-TMI retrieval database is built up with PR profiles, PR and TMI errors will be compared to assess the extent PR error could affect BRAIN-TMI retrievals.

The satellite rainfall estimate errors are represented by the residuals between satellite rainfall estimates and reference GV as expressed by Eq. (1). Based on the previous considerations, conditional probability distribution functions of satellite QPE errors ε are built. First, the rain intensity R_{ref} is tested as the main driving variable conditioning the departures of satellite-based estimates from GV. Given the nonlinearities of the satellite error, the variability that may result from the observed atmosphere and the sensors, and the non-Gaussian distribution of errors, the conditional distributions of the residuals, denoted $f(\varepsilon|R_{\text{ref}})$, are analysed within the framework of the so-called Generalized Additive Models for Location, Scale and Shape proposed by Rigby and Stasinopoulos (2005). This tool is available in an R package called GAMLSS (Stasinopoulos and Rigby, 2007). In this framework, the response variable is ε and the explanatory variable is R_{ref} . We assume that $f(\varepsilon|R_{\text{ref}})$ has the same parametric form for all R_{ref} values. For the sake of simplicity and to distinguish between systematic and random errors in satellite rainfall estimates, a number of conditional densities parametrized with the first two moments (the location μ – mean, to be linked to systematic errors – and the scale σ – standard deviation representative of random errors) are considered here. The first two moments as functions of the explanatory variable R_{ref} characterise the conditional distributions of satellite residuals.

GAMLSS models the parameters of a response variable's distribution. Such semi-parametric models consist of two components: a parametric probability density function (PDF) given each value of the explanatory variable and a non-parametric relationship between the PDF parameters (μ, σ) over the definition domain of the explanatory variable. Two main assumptions are made: (i) the response variable ε is a random variable following a known parametric distribution with density $f(\varepsilon|\mu, \sigma)$ conditional on the parameters (μ, σ); and (ii) the observations ε are mutually independent given the parameter vectors (μ, σ). Each parameter is modelled as a function of R_{ref} (the explanatory variable) using monotonic (linear/nonlinear or smooth) link functions. More details are provided by Rigby and Stasinopoulos (2001, 2005), Akantziliotou *et al.* (2002) and Stasinopoulos and Rigby (2007). The rainfall trends for each parameter are fitted using locally weighted scatterplot smoothing (LOESS), which are more flexible than polynomials or fractional polynomials for modelling complex nonlinear relationships. The polynomial curve is determined by R_{ref} and fitted locally by weighted polynomial regression, giving more weight to points near the point whose response is being estimated and less weight to points further away (Cleveland *et al.*, 1993). A trade-off between over- and under-smoothing is found

Table 11. Performance criteria values for PR and BRAIN-TMI estimates.

PR	Benin		Niger	
	PR resampled (whole) robust GV	PR >0.3	Robust GV	PR >0.3
Mean (mm h ⁻¹)	4.52 (4.09)	3.77 (3.24)	3.29 (4.49)	3.43 (3.76)
standard deviation (mm h ⁻¹)	6.39	4.49	4.51	3.56
MRE/GV (%)	–	–16% (–21%)	–	4% (–16%)
Correlation/GV	–	0.52	–	0.40
BRAIN-TMI	Benin		Niger	
	BRAIN-TMI robust GV	BRAIN-TMI	Robust GV	BRAIN-TMI
Mean (mm h ⁻¹)	5.59	4.92	6.68	7.3
standard deviation (mm h ⁻¹)	7.97	4.4	9.2	6.39
MRE/GV (%)	–	–12%	–	9%
Correlation/GV	–	0.24	–	0.41

Mean, standard deviation, mean relative error (MRE) and correlation (R) are given with respect to GV. These criteria are given for the Benin and Niger areas. In addition, the climatological means and MRE are also provided when PR is compared with the whole GV dataset (brackets). Only the ‘robust’ GV data are kept (see section 2.2) for GV and only the rain intensities >0.3 mm h⁻¹ are kept for PR.

following the procedure described by Stasinopoulos and Rigby (2007). Several two-parameter density functions (log-normal, normal, reverse Gumbel, logistic, gamma, etc.) have been tested to fit the data. The distributions of residuals (not shown here) were generally found to be unimodal and asymmetric. The goodness-of-fit on the whole dataset has been checked using the Akaike information criteria (AIC, a penalised function of the log-likelihood function to be minimised in the fitting procedure) for each semi-parametric density fit. The reverse Gumbel distribution ($f(\varepsilon) = \frac{1}{\sigma} \left[-\left(\frac{\varepsilon-\mu}{\sigma}\right) - \exp\left\{-\left(\frac{\varepsilon-\mu}{\sigma}\right)\right\} \right]$, where μ is the mean and σ the standard deviation of the residual population) was found to present the best fit. Figure 10 shows the residuals as a function of R_{ref} as well as the fitted GAM models for PR and BRAIN-TMI over Benin and Niger. The conditional PDFs of residuals present a high conditional shift from the zero line (conditional median shifted from the zero line) and a high conditional spread. Note that for $R_{\text{ref}} > 10$ mm h⁻¹, the models are quite undefined because of the lack of observed residuals. All models show that PR and BRAIN-TMI tend to overestimate light rain rates (the median of residuals is positive) and underestimate higher rain rates (median of residuals negative). In order to compare BRAIN-TMI and PR over the two areas, we extracted the systematic error component (i.e. conditional bias). Because the conditional density of residuals is non-symmetric, we used the median rather than the expectation for a better representation of this conditional bias. This is shown as a function of R_{ref} for PR and BRAIN-TMI over Benin and Niger in Figure 11. The overestimation of light rain rates is more significant for BRAIN-TMI than for PR and in Niger than in Benin (as shown in sections 3.2 and 3.4): e.g. in Benin BRAIN-TMI overestimates $R_{\text{ref}} = 2$ mm h⁻¹ rain rates with an occurrence of 90% and with a representative bias of +2 mm h⁻¹ while PR overestimates the same rain rates with an occurrence of 70% and with a representative bias of +0.5 mm h⁻¹. The overestimation affects a larger range of rain rates for BRAIN-TMI than for PR and in Niger than in Benin. The median of residuals is equal to 0 at 4 mm h⁻¹ and 4.5 mm h⁻¹ for PR in Benin and Niger respectively, while the median of residuals is equal to 0 at 5 mm h⁻¹ and 6.5 mm h⁻¹ for BRAIN-TMI in Benin and Niger respectively. Globally the PR performs better than BRAIN-TMI in reproducing the lighter rain rates (as shown in section 3.2) with limited overestimation. The

PR bias at higher rain rates is more significant. While the bias is within +1 mm h⁻¹ in both regions for $R_{\text{ref}} < 4$ mm h⁻¹, it decreases continuously for $R_{\text{ref}} > 4$ mm h⁻¹ to reach –5 mm h⁻¹ at $R_{\text{ref}} = 10$ mm h⁻¹. Once again, this is likely due to the insufficient correction of PR attenuation for heavier rain rates. For BRAIN-TMI the overall bias relative to GV in Benin and Niger is low (see section 3.4) because of the balance between the overestimation of light rain rates and the underestimation of high rain rates.

It is worth noting that BRAIN-TMI is less biased than PR for the higher rain rates. As the BRAIN-TMI retrieval database is built up with PR profiles, at least as much underestimation from BRAIN-TMI as for PR could be expected. An inquiry to the BRAIN-TMI database revealed that some PR profiles link high rainfall rates and low brightness temperatures at 85 GHz and 37 GHz, and contribute to the retrievals of BRAIN-TMI in highly rainy situations, but these profiles are not from the African region. In the retrieval database design a number of inconsistencies between brightness temperatures and PR surface rain were encountered. This was generally associated with (i) situations when the PR profile could be insufficiently corrected for attenuation in cases of heavy rain rates (light surface rain with very cold 85 GHz brightness temperature), and (ii) cold 85 GHz T_{bs} may not be associated with heavy surface rainfall due to the satellite parallax and vertical shear (for very deep convection, the surface location and corresponding PR profile of the TMI footprint may be displaced 8 km from the footprint at cloud top). These profiles were discarded from the database, hopefully limiting the bias due to inadequate correction for attenuation losses of the PR radar signal in BRAIN-TMI.

For both BRAIN-TMI and PR, we finally quantify the contribution of the rain rate-dependent biases to the residuals. For each BRAIN-TMI or PR measurement, we use the model of rain rate-conditioned bias (Figure 11) to simulate the systematic bias corresponding to each residual ε and reference R_{ref} . For each sensor and GV domain the series of observed residual ε is compared to the series of conditional bias. A determination coefficient computed between the two samples provides the proportion of variability in the residual sample explained by the conditional bias. The results show that 66% and 52% of the variance of the residuals is explained by the systematic error for BRAIN-TMI over Benin and

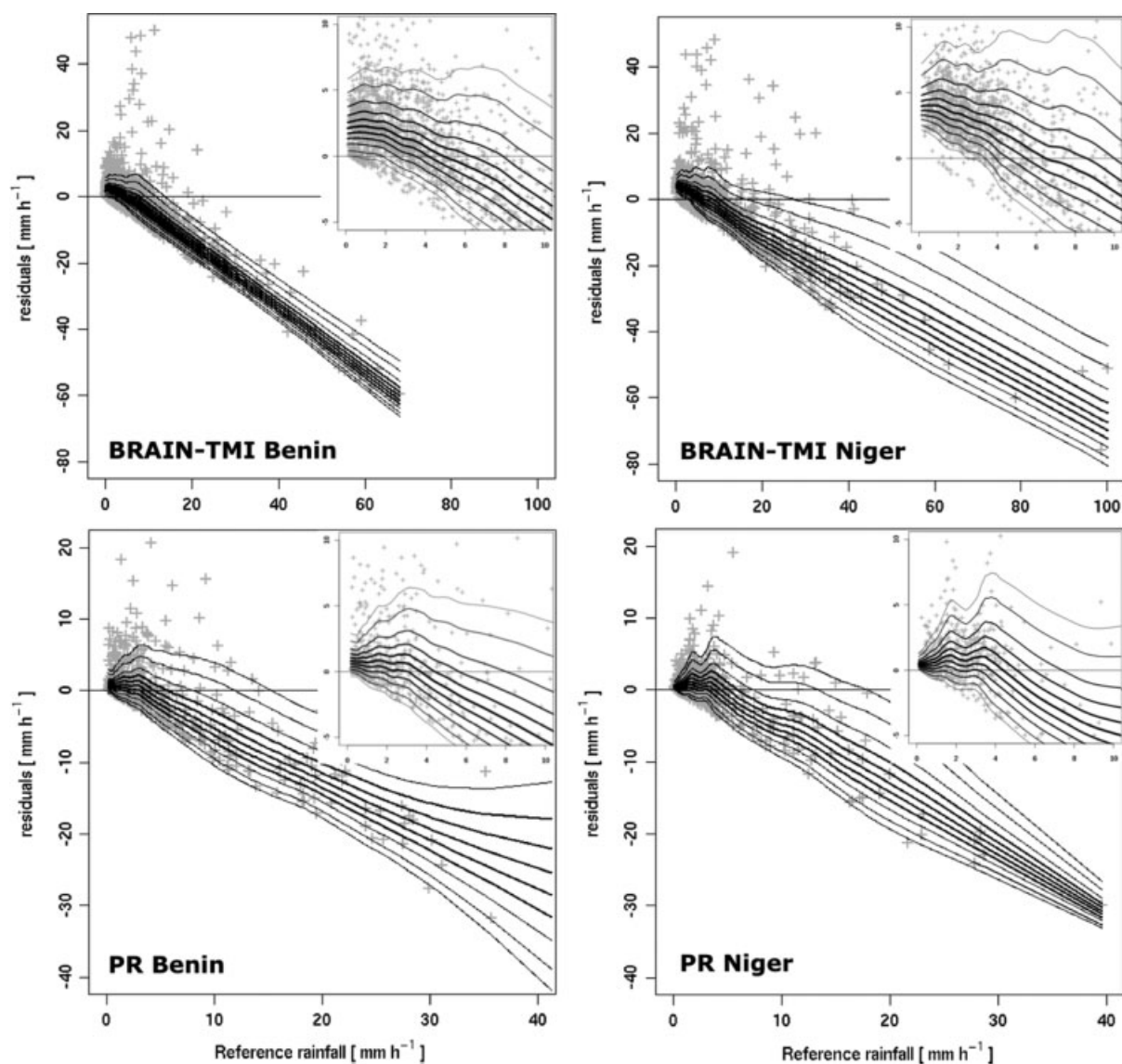


Figure 10. Satellite-based residuals represented versus GV for (top) BRAIN-TMI and (bottom) PR, over (left) Benin and (right) Niger; the GAM models fitted are represented by 5, 10, 20, 30, 40, 50, 60, 70, 80, 90 and 95 percentile lines.

Niger respectively, while 47% and 30% of the variance of the residuals is explained by the systematic error for PR over Benin and Niger respectively. This confirms that a significant amount of BRAIN-TMI error is due to conditional biases of the algorithm. The amount shows a regional dependence (lower proportion of variability explained in Niger than in Benin), which may be related to the rainfall regime. In fact, residuals depend as much on the systematic biases of satellite-based estimates as on the spread of the GV rainfall distribution. The standard deviation of the GV rainfall distribution in Niger being greater than in Benin (Table 11), it is consistent that the contribution of satellite-based systematic biases to residuals is lower in Niger than in Benin.

5. Conclusions

In preparation for the Megha-Tropiques mission, the BRAIN algorithm was evaluated using ten-year data samples from the TRMM satellite passive microwave imager, active PR rainfall products and surface rainfall derived from rain-gauges over West Africa. The ability of space-based rain

retrievals to reproduce the differences of rainfall regimes in Benin and Niger has been investigated to characterise the satellite error estimate. The comparison has been performed at the microwave satellite resolution to avoid additional uncertainties by resampling. This is appropriate to qualitatively and quantitatively assess the retrieval uncertainties. A framework has been proposed to address methodological issues so as to provide a preliminary version of an error model for satellite instantaneous QPEs. The error model is empirically derived and thus prone to be specific to the dataset considered and the satellite data processing implemented. Several factors limit the comparison samples for ground-based and satellite-based estimates over the 10-year period, especially for the PR comparison dataset. In spite of the possible lack of robustness for the statistics considered, the features of the error model are quite representative as they show a consistent behaviour in terms of conditioning with respect to rain rate.

Sampling uncertainty in the GV is confirmed to be an issue for quantitative assessment of satellite products. Here 'robust' GV pixels were selected based on the value of the kriging variance relative to the estimate. The finding is

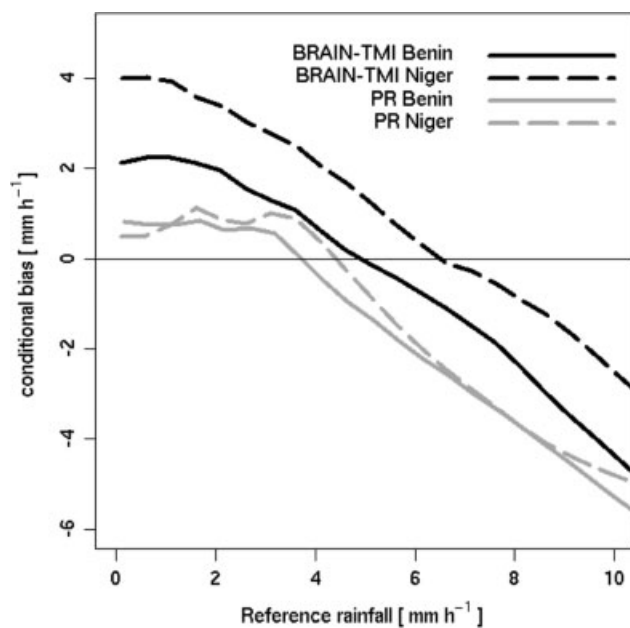


Figure 11. Conditional median of residuals as a function of GV for BRAIN-TMI (black lines) and PR (grey lines), over Benin (solid lines) and Niger (dotted lines).

that apparent misses in the satellite products are mainly associated with GV pixels of high uncertainty; when the comparison is limited to 'robust' GV points, the scores are greatly improved.

Rainfall estimates from the three sensors show very consistent features over the two mesoscale sites. BRAIN-TMI and PR exhibit the differences in rain-rate distributions and spatial structures between North Benin (Sudanese ecoclimatic zone) and Niger (Sahelian zone). Different error sources were identified and quantified for BRAIN-TMI:

- Rain/no-rain delineation is suspected to cause the most significant error. It was estimated that at least 20% of the rainfall volume is lost this way. The rain mask fails to detect the lightest rain rates and the most inhomogeneous parts of rain fields. Nevertheless, variogram analysis showed the mask is sufficient to capture the spatial structure of the rainiest and most organised parts of rain fields.
- Within the rain mask, BRAIN-TMI presents a narrow and low-biased PDF relative to GV; it smooths rain-rate dynamics, which may be an effect of the Bayesian scheme used.
- Designed to provide low overall biased retrievals, BRAIN-TMI correctly estimates (with around 10% accuracy) the interannual mean rainfall values over the two areas.
- Finally, when adding the overall bias of retrievals and the systematic misses of rain volume, the underestimation of BRAIN is roughly 30% over Benin (the volume of the not-detected rainfall adds up with underestimation in the retrievals) and 10% over Niger (the missed volume is compensated by overestimation in the retrievals).

The PR was also compared with the GV to see if the PR could be used as a reference to validate BRAIN-TMI. Good convergence between PR and GV was found in terms of contingency. While PR does not detect very light events

(<0.3 mm h⁻¹), it may be used as reference to evaluate the BRAIN-TMI rain/no-rain mask. It seems difficult to use PR distribution as a reference to evaluate BRAIN-TMI distribution since PR significantly underestimates high rain rates. To validate BRAIN-TMI variograms we suggest computing PR variograms within the BRAIN-TMI mask.

Finally, a statistical model that describes BRAIN-TMI (and PR) uncertainty was developed. It quantifies the relation between instantaneous satellite rainfall and the corresponding reference rainfall. It consists of a deterministic additive function and a random uncertainty component, both conditioned on GV rain rate. The analysis over the two GV sites showed a dependence on the rain type (deep convection in Niger versus various convection types in Benin). The contribution of systematic BRAIN-TMI algorithm errors is confirmed to be quite large. They probably arise from the physical inconsistency and/or non-representativeness of the cloud-radiative-model-simulated profiles that support the algorithm. This type of error is not related to the sampling error, and further research must be done to determine its relative contribution to the total error in space-based precipitation estimates.

Further work will address the relative contributions of errors resulting from uncertainties in PR estimates, spatial sampling mismatches, and errors in cloud radiative modelling. The same is true for the influence of the rainfall type. Further research is necessary to improve the rain/no-rain detection for BRAIN-TMI. Another important issue to study is how the various error sources (misses, conditional biases) propagate when merging with geostationary infrared data for a number of satellite-based high-resolution precipitation products.

Acknowledgements

The critical comments of two anonymous reviewers were very helpful for improving the manuscript. The ground data were provided by the AMMA-CATCH observing system; we are very much indebted to the crew that operated the AMMA-CATCH ground networks and processed the rain data, especially Julien Viarre and Guillaume Quantin. Based on a French initiative, AMMA (African Monsoon Multidisciplinary Analyses) was developed by an international scientific group and is currently funded by a large number of agencies, especially from France, UK, USA and Africa. It has been the beneficiary of a major financial contribution from the European Community's Sixth Framework Research Programme. The research presented in this paper was funded by a post-doctoral grant from the Centre National d'Études Spatiales. We thank Tioka Tokedira for kindly proof-reading the English language.

References

- Adeyewa ZD, Nakamura K. 2003. Validation of TRMM radar rainfall data over major climatic regions in Africa. *J. Appl. Meteorol.* **42**: 331–347.
- Akantziliotou K, Rigby RA, Stasinopoulos DM. 2002. 'The R implementation of Generalized Additive Models for Location, Scale and Shape.' Pp 75–83 in *Statistical modelling in Society: Proc. 17th International Workshop on statistical modelling, Chania, Greece*. Stasinopoulos M, Touloumi G (eds).
- Andersen J, Dybkjaer G, Jensen KH, Refsgaard JC, Rasmussen K. 2002. Use of remotely sensed precipitation and leaf area index in a distributed hydrological model. *J. Hydrol.* **264**: 34–50.

- Amitai E, Lloret X, Sempere-Torres D. 2006. Opportunities and challenges for evaluating precipitation estimates during GPM mission. *Meteorol. Z.* **15**: 551–557.
- Amitai E, Lloret X, Sempere-Torres D. 2009. Comparison of TRMM radar rainfall estimates with NOAA Next-Generation QPE. *J. Meteorol. Soc. Jpn* **87A**: 109–118.
- Bergès JC, Jobard I, Chopin F, Roca R. 2010. EPSAT-SG: A satellite method for precipitation estimation; its concepts and implementation for the AMMA experiment. *Ann. Geophys.* **28**: 289–308.
- Chambon P, Jobard I, Roca R, Viltard N. 2012. An investigation of the error budget of tropical rainfall accumulation derived from merged passive microwave and infrared satellite measurements. *Q. J. R. Meteorol. Soc.*, DOI: 10.1002/qj.1907.
- Ciach GJ. 2003. Local random errors in tipping-bucket rain gauge measurements. *J. Atmos. Oceanic Technol.* **20**: 752–759.
- Ciach GJ, Krajewski WF. 1999. On the estimation of radar rainfall error variance. *Adv. Water Resour.* **22**: 585–595.
- Ciach GJ, Habib E, Krajewski WF. 2003. Zero-covariance hypothesis in the error variance separation method of radar rainfall verification. *Adv. Water Resour.* **26**: 573–580.
- Cleveland WS, Grosse E, Shyu M. 1993. Local regression models. Pp 309–376 in *Statistical Models in S*, Chambers JM, Hastie TJ (eds). Chapman & Hall: New York, NY.
- Conway D, Persechino A, Ardoin-Bardin S, Hamandawana H, Dieulin C, Mahé G. 2009. Rainfall and water resources variability in sub-Saharan Africa during the twentieth century. *J. Hydrometeorol.* **10**: 41–59.
- D'Amato N, Lebel T. 1998. On the characteristics of the rainfall events in the Sahel with a view to the analysis of climatic variability. *Int. J. Climatol.* **18**: 955–974.
- Depraetere C, Gosset M, Ploix S, Laurent H. 2009. The organization and kinematics of tropical rainfall systems ground tracked at mesoscale with gauges: First results from the campaigns 1999–2006 on the Upper Ouémé Valley (Benin). *J. Hydrol.* **375**: 143–160.
- Ebert E. 2007. Methods for verifying satellite precipitation estimates. Pp 345–356 in *Measuring Precipitation from Space: EURAINSAT and the future*, Levizzani V, Bauer P, Turk FJ (eds). Springer.
- Geerts B, Dejene T. 2005. Regional and diurnal variability of the vertical structure of precipitation systems in Africa based on spaceborne radar data. *J. Climate* **18**: 893–916.
- Grimes DIF, Diop M. 2003. Satellite-based rainfall estimation for river flow forecasting in Africa. I: Rainfall estimates and hydrological forecasts. *Hydrol. Sci. J.* **48**: 567–584.
- Habib E, Ciach GJ, Krajewski WF. 2004. A method for filtering out rain gauge representativeness errors from the verification distributions of radar and rain gauge rainfall. *Adv. Water Resour.* **27**: 967–980.
- Iguchi T, Kozu T, Meneghini R, Awaka J, Okamoto K. 2000. Rain-profiling algorithm for the TRMM precipitation radar. *J. Appl. Meteorol.* **39**: 2038–2052.
- Journal AG, Huijbregts CJ. 1978. *Mining Geostatistics*. Academic Press: London.
- Kirstetter P-E, Delrieu G, Boudevillain B, Obled C. 2010. Toward an error model for radar quantitative precipitation estimation in the Cévennes–Vivarais region, France. *J. Hydrol.* **394**: 28–41.
- Kummerow C, Barnes W, Kozu T, Shiue J, Simpson J. 1998. The Tropical Rainfall Measuring Mission (TRMM) sensor package. *J. Atmos. Oceanic Technol.* **15**: 809–817.
- Kummerow C, Berg W, Thomas-Stahle J, Masunaga H. 2006. Quantifying global uncertainties in a simple microwave rainfall algorithm. *J. Atmos. Oceanic Technol.* **23**: 23–37.
- Lebel T, Amani A. 1999. Rainfall estimation in the Sahel: What is the ground truth?. *J. Appl. Meteorol.* **38**: 555–568.
- Lebel T, Bastin G, Obled C, Creutin JD. 1987. On the accuracy of areal rainfall estimation: A case study. *Water Resour. Res.* **23**: 2123–2134.
- Lebel T, Cappelaere C, Galle S, Hanan N, Kergoat L, Levis S, Vieux B, Descroix L, Gosset M, Mougin E, Peugeot C, Seguis L. 2009. AMMA-CATCH studies in the Sahelian region of West-Africa: An overview. *J. Hydrol.* **375**: 3–13.
- Lebel T, Parker DJ, Flamant C, Bourlès B, Marticorena B, Mougin E, Peugeot C, Diedhiou A, Haywood JM, Ngamini JB, Polcher J, Redelsperger J-L, Thorncroft CD. 2010. The AMMA field campaigns: Multiscale and multidisciplinary observations in the West African region. *Q. J. R. Meteorol. Soc.* **136**(S1): 8–33.
- L'ecuyer TS, Stephens GL. 2002. An uncertainty model for Bayesian Monte Carlo retrieval algorithms: Application to the TRMM observing system. *Q. J. R. Meteorol. Soc.* **128**: 1713–1737.
- Leroux M. 2001. *The Meteorology and Climate of Tropical Africa*. Springer-Verlag.
- Lin X, Hou AY. 2008. Evaluation of coincident passive microwave rainfall estimates using TRMM PR and ground measurements as references. *J. Appl. Meteorol. Clim.* **47**: 3170–3187.
- Nicholson SE, Some B, Kone B. 2000. An analysis of recent rainfall conditions in West Africa, including the rainy seasons of the 1997 El Niño and the 1998 La Niña years. *J. Climate* **13**: 2628–2640.
- Nicholson SE, Some B, McCollum J, Nelkin E, Klotter D, Berte Y, Diallo BM, Gaye I, Kpabeba G, Ndiaye O, Noukpozoukou JN, Tanu MM, Thiam A, Toure AA, Traore AK. 2003a. Validation of TRMM and other rainfall estimates with a high-density gauge dataset for West Africa. Part I: Validation of GPCC rainfall product and pre-TRMM satellite and blended products. *J. Appl. Meteorol.* **42**: 1337–1354.
- Nicholson SE, Some B, McCollum J, Nelkin E, Klotter D, Berte Y, Diallo BM, Gaye I, Kpabeba G, Ndiaye O, Noukpozoukou JN, Tanu MM, Thiam A, Toure AA, Traore AK. 2003b. Validation of TRMM and other rainfall estimates with a high-density gauge dataset for West Africa. Part II: Validation of TRMM rainfall products. *J. Appl. Meteorol.* **42**: 1355–1368.
- Redelsperger J-L, Diongue A, Diedhiou A, Ceron J-P, Diop M, Gueremy J-F, Lafore J-P. 2002. Multi-scale description of a Sahelian synoptic weather system representative of the West African monsoon. *Q. J. R. Meteorol. Soc.* **128**: 1229–1257.
- Redelsperger J-L, Thorncroft CD, Diedhiou A, Lebel T, Parker DJ, Polcher J. 2006. African Monsoon Multidisciplinary Analysis: An international research project and field campaign. *Bull. Am. Meteorol. Soc.* **87**: 1739–1746.
- Rigby RA, Stasinopoulos DM. 2001. 'The GAMLSS project: A flexible approach to statistical modelling.' Pp 249–256 in *New Trends in Statistical Modelling*, Klein B, Korsholm L (eds). Proc. 16th International Workshop on statistical modelling, Odense, Denmark, 2–6 July 2001.
- Rigby RA, Stasinopoulos DM. 2005. Generalized additive models for location, scale and shape. *Appl. Stat.-J. Roy. St. C* **54**: 507–554.
- Roca R, Chambon P, Jobard I, Kirstetter P-E, Gosset M, Bergès JC. 2010. Comparing satellite and surface rainfall products over West Africa at meteorologically relevant scales during the AMMA campaign using error estimates. *J. Appl. Meteorol. Clim.* **49**: 715–731.
- Sapiano MRP, Arkin PA. 2009. An intercomparison and validation of high-resolution satellite precipitation estimates with 3-hourly gauge data. *J. Hydrometeorol.* **10**: 149–166.
- Schumacher C, Houze Jr RA. 2000. Comparison of radar data from the TRMM satellite and Kwajalein oceanic validation site. *J. Appl. Meteorol.* **39**: 2151–2164.
- Stasinopoulos DM, Rigby RA. 2007. Generalized Additive Models for Location Scale and Shape (GAMLSS) in R. *J. Stat. Softw.* **10**: 1–46.
- Stephens GL, Kummerow CD. 2007. The remote sensing of clouds and precipitation from space: A review. *J. Atmos. Sci.* **64**: 3742–3765.
- Turk FJ, Arkin P, Sapiano MRP, Ebert EE. 2008. Evaluating high-resolution precipitation products. *Bull. Am. Meteorol. Soc.* **89**: 1911–1916.
- Ushio T, Okamoto K, Kubota T, Hashizume H, Shige S, Noda S, Iida Y, Aonashi K, Inoue T, Oki R, Kachi M, Takahashi N, Iguchi T. 2006. 'A combined microwave and infrared radiometer approach for a high resolution global precipitation mapping in the GSMaP project Japan.' 3rd Int. Precipitation Working Group Workshop on precipitation measurements, Melbourne, Australia.
- Viltard N, Kummerow C, Olson WS, Hong Y. 2000. Combined use of the radar and radiometer of TRMM to estimate the influence of drop size distribution on rain retrievals. *J. Appl. Meteorol.* **39**: 2103–2114.
- Viltard N, Burlaud C, Kummerow CD. 2006. Rain retrieval from TMI brightness temperature measurements using a TRMM PR-based database. *J. Appl. Meteorol. Clim.* **45**: 455–466.
- Vischel T, Quantin G, Lebel T, Viarre J, Gosset M, Cazenave F, Panthou G. 2011. Generation of high-resolution rain fields in West Africa: Evaluation of dynamic interpolation methods. *J. Hydrometeorol.* **12**: 1465–1482.
- Wilheit T, Kummerow CD, Ferraro R. 2003. Rainfall algorithms for AMSR-E. *IEEE Trans. Geosci. Remote Sensing* **41**: 204–214.
- Wolff DB, Fisher BL. 2008. Comparisons of instantaneous TRMM ground validation and satellite rain-rate estimates at different spatial scales. *J. Appl. Meteorol. Clim.* **47**: 2215–2237.
- Wolff DB, Fisher BL. 2009. Assessing the relative performance of microwave-based satellite rain-rate retrievals using TRMM ground validation data. *J. Appl. Meteorol. Clim.* **48**: 1069–1099.
- Xu XY, Howard K, Zhang J. 2008. An automated radar technique for the identification of tropical precipitation. *J. Hydrometeorol.* **9**: 885–902.
- Yang S, Olson WS, Wang J-J, Bell TL, Smith EA, Kummerow CD. 2006. Precipitation and latent heating distributions from satellite passive microwave radiometry. Part II: Evaluation of estimates using independent data. *J. Appl. Meteorol. Clim.* **45**: 721–739.
- Zeweldi DA, Gebremichael M. 2009. Sub-daily scale validation of satellite-based high-resolution rainfall products. *Atmos. Res.* **92**: 427–433.